



University of Kentucky  
UKnowledge

---

Theses and Dissertations--Rehabilitation  
Sciences

College of Health Sciences

---

2020

## TRANSCRIPTOMIC AND CELLULAR RESPONSE TO MECHANICAL OVERLOAD AND THE UNDERLYING ROLE OF MACROPHAGES IN EXTRACELLULAR MATRIX REMODELING

Bailey D. Peck

University of Kentucky, [bailey.peck@uky.edu](mailto:bailey.peck@uky.edu)

Digital Object Identifier: <https://doi.org/10.13023/etd.2020.514>

[Right click to open a feedback form in a new tab to let us know how this document benefits you.](#)

### Recommended Citation

Peck, Bailey D., "TRANSCRIPTOMIC AND CELLULAR RESPONSE TO MECHANICAL OVERLOAD AND THE UNDERLYING ROLE OF MACROPHAGES IN EXTRACELLULAR MATRIX REMODELING" (2020). *Theses and Dissertations--Rehabilitation Sciences*. 74.  
[https://uknowledge.uky.edu/rehabsci\\_etds/74](https://uknowledge.uky.edu/rehabsci_etds/74)

This Doctoral Dissertation is brought to you for free and open access by the College of Health Sciences at UKnowledge. It has been accepted for inclusion in Theses and Dissertations--Rehabilitation Sciences by an authorized administrator of UKnowledge. For more information, please contact [UKnowledge@lsv.uky.edu](mailto:UKnowledge@lsv.uky.edu).

## **STUDENT AGREEMENT:**

I represent that my thesis or dissertation and abstract are my original work. Proper attribution has been given to all outside sources. I understand that I am solely responsible for obtaining any needed copyright permissions. I have obtained needed written permission statement(s) from the owner(s) of each third-party copyrighted matter to be included in my work, allowing electronic distribution (if such use is not permitted by the fair use doctrine) which will be submitted to UKnowledge as Additional File.

I hereby grant to The University of Kentucky and its agents the irrevocable, non-exclusive, and royalty-free license to archive and make accessible my work in whole or in part in all forms of media, now or hereafter known. I agree that the document mentioned above may be made available immediately for worldwide access unless an embargo applies.

I retain all other ownership rights to the copyright of my work. I also retain the right to use in future works (such as articles or books) all or part of my work. I understand that I am free to register the copyright to my work.

## **REVIEW, APPROVAL AND ACCEPTANCE**

The document mentioned above has been reviewed and accepted by the student's advisor, on behalf of the advisory committee, and by the Director of Graduate Studies (DGS), on behalf of the program; we verify that this is the final, approved version of the student's thesis including all changes required by the advisory committee. The undersigned agree to abide by the statements above.

Bailey D. Peck, Student

Dr. Charlotte A. Peterson, Major Professor

Dr. Esther E. Dupont-Versteegden, Director of Graduate Studies

TRANSCRIPTOMIC AND CELLULAR RESPONSE TO MECHANICAL  
OVERLOAD AND THE UNDERLYING ROLE OF MACROPHAGES IN  
EXTRACELLULAR MATRIX REMODELING

---

DISSERTATION

---

A dissertation submitted in partial fulfillment of the  
requirements for the degree of Doctor of Philosophy in the  
College of Health Sciences  
at the University of Kentucky

By

Bailey Dakota Peck  
Lexington, Kentucky

Co-Directors: Dr. Charlotte Peterson, Professor of Rehabilitation Health Sciences and  
Dr. Esther Dupont-Versteegden, Professor of Rehabilitation Health Sciences  
Lexington, Kentucky

2020

Copyright © Bailey Dakota Peck 2020

## ABSTRACT OF DISSERTATION

### TRANSCRIPTOMIC AND CELLULAR RESPONSE TO MECHANICAL OVERLOAD AND THE UNDERLYING ROLE OF MACROPHAGES IN EXTRACELLULAR MATRIX REMODELING

The extracellular matrix (ECM) in skeletal muscle plays an integral role in tissue development, structural support, and force transmission. Upon mechanical loading, including resistance exercise, which alter muscle fiber contractile activity, size, orientation and connectivity, remodeling processes must occur that involve both ECM deposition and degradation. ECM remodeling involves many cell types in muscle, but the focus of our research was directed towards macrophages, which participate in the early immune response to damage and loading. We have consistently demonstrated a significant increase in skeletal muscle macrophage abundance using pan macrophage markers (CD11b/CD68) and anti-inflammatory markers (CD206/CD163) following exercise training in both middle aged and older adults. We report that with 14-weeks of progressive resistance exercise training (PRT) in older adults (>65 years of age), genes involved in ECM remodeling, including *MMP14*, a master regulator of ECM turnover, were the most upregulated, differentially expressed genes among those identified by RNA-sequencing in muscle biopsies. Following an acute bout of resistance exercise in humans and mechanical overload in mouse, single cell RNA-sequencing indicated that muscle macrophages accumulate *MMP14* mRNA. In vitro, we identified leukemia inhibitory factor (LIF), secreted by electrically-stimulate primary human myotubes, as a contributor to upregulation of *MMP14* expression in macrophages. The data presented identify a novel mechanism by which skeletal muscle and macrophages interact to promote ECM remodeling in response to mechanical overload.

**KEYWORDS:** Macrophages, Skeletal Muscle, Mechanical Overload, Extracellular Matrix Remodeling, Transcriptomics, Single Cell RNA-sequencing

Bailey Dakota Peck  
*(Name of Student)*

---

10/07/2020  
Date

---

TRANSCRIPTOMIC AND CELLULAR RESPONSE TO MECHANICAL  
OVERLOAD AND THE UNDERLYING ROLE OF MACROPHAGES IN  
EXTRACELLULAR MATRIX REMODELING

By  
Bailey Dakota Peck

Dr. Charlotte Peterson

---

Co-Director of Dissertation

Dr. Esther Dupont-Versteegden

---

Co-Director of Dissertation

Dr. Esther Dupont-Versteegden

---

Director of Graduate Studies

10/07/2020

---

Date

## TABLE OF CONTENTS

<i>LIST OF FIGURES</i> .....	v
<i>LIST OF ADDITIONAL FILES</i> .....	vi
<i>CHAPTER 1. Introduction to skeletal muscle macrophages and extracellular matrix remodeling with mechanical overload</i> .....	1
1.1 Skeletal muscle extracellular matrix and regulators of remodeling.....	1
1.2 Macrophage characterization and activation .....	2
1.3 Evidence of macrophage contribution to ECM deposition .....	4
1.4 Evidence of macrophage contribution to ECM degradation.....	5
1.5 Adverse effects of macrophage depletion on skeletal muscle adaptations following damage in mice.....	6
1.6 Deficits in muscle growth and regrowth with macrophage depletion in mice ...	8
1.7 Macrophages in human skeletal muscle adaptation .....	9
1.8 Skeletal muscle influence on macrophage activation state .....	10
1.9 Preview of studies presented.....	10
<i>CHAPTER 2. Metformin alters skeletal muscle transcriptome adaptations to resistance training in older adults</i> .....	12
2.1 Introduction .....	12
2.2 Methods.....	15
2.2.1 Study Design, Participants and Interventions .....	15
2.2.2 Library Preparation .....	16
2.2.3 Sequencing, Preprocessing and Alignment.....	17
2.2.4 Differential Gene Expression Analysis.....	17
2.2.5 Pathway Overrepresentation Analysis .....	18
2.2.6 Data availability statement.....	19
2.3 Results.....	19
2.3.1 Global gene expression changes in skeletal muscle with placebo + progressive resistance training (plaPRT) or metformin + progressive resistance training (metPRT) .....	19
2.3.2 Pathway overrepresentation within differentially expressed genes (DEG) .....	20
2.3.3 Reversal of the aging skeletal muscle transcriptome with PRT and metformin.....	21
2.4 Discussion .....	22
<i>CHAPTER 3. Macrophage contribution to extracellular matrix remodeling with mechanical overload</i> .....	30

3.1	Introduction.....	30
3.2	Methods.....	33
3.2.1	Human subjects and intervention.....	33
3.2.2	Muscle Biopsies .....	34
3.2.3	Animals .....	34
3.2.4	Synergist ablation surgery-induced mechanical overload (MOV) of muscle .....	34
3.2.5	Mononuclear cell isolation from skeletal muscle .....	35
3.2.6	Cell Culture .....	35
3.2.7	DQ collagen type I assay .....	36
3.2.8	Immunohistochemistry .....	37
3.2.9	Gene expression experiments in myotubes and BMDM .....	39
3.2.10	Single cell RNA-sequencing (scRNA-seq).....	40
3.2.11	Statistical Analyses .....	41
3.3	RESULTS .....	42
3.3.1	The increase in human muscle macrophages following PRT is positively associated with changes in muscle fiber cross-sectional area (CSA), capillary density, myonuclear accretion and satellite cell abundance .....	42
3.3.2	Human skeletal muscle macrophage scRNA-seq transcriptome changes following an acute bout of resistance exercise (RE).....	43
3.3.3	Mouse MOV induced changes in macrophage sub-populations, activation and <i>MMPI4</i> expression.....	44
3.3.4	LIF mediates increases in <i>MMPI4</i> expression in bone marrow derived macrophages (BMDM) in response to EPS-stimulated myotube conditioned media (CM) .....	46
3.3.5	BMDM treated with EPS conditioned media display enhanced type I collagen degradation .....	47
3.4	Discussion.....	48
	<i>CHAPTER 4. Concluding remarks and future directions .....</i>	<i>63</i>
4.1	Summary of findings regarding the regulation of ECM with MOV.....	63
4.2	Is ECM turnover necessary for skeletal muscle adaptations to MOV? .....	64
4.3	Skeletal muscle and muscle macrophage crosstalk validation in vivo .....	64
4.4	Macrophage ablation models to demonstrate global impact with MOV .....	65
4.5	Final Remarks .....	65
	<i>REFERENCES .....</i>	<i>67</i>
	<i>VITA .....</i>	<i>75</i>



## LIST OF FIGURES

Figure 2.1 Metformin blunts the global transcriptomic changes induced by PRT in human skeletal muscle. ....	27
Figure 2.2 Pathway overrepresentation analyses on differentially expressed genes (DEG). ....	28
Figure 2.3 PRT reverts aging transcriptome towards that of young resting muscle and the effects of metformin are additive. ....	29
Figure 3.1 Correlations between changes in skeletal muscle plasticity and macrophages	54
Figure 3.2 Representative images of skeletal muscle immunohistochemistry. ....	55
Figure 3.3 scRNA-seq of CD11b+/CD45+ sorted cells derived from human <i>vastus lateralis</i> 24 hr after an acute bout of RE. ....	56
Figure 3.4 scRNA-seq analysis of growth factors identified in human macrophages .....	57
Figure 3.5 scRNA-seq demonstrates dynamic changes in cell populations following 4 days of mechanical overload (MOV) in mouse plantaris. ....	58
Figure 3.6 scRNA-seq of mouse macrophage populations under Sham and mechanical overload (MOV) conditions. ....	60
Figure 3.7 BMDM require LIF upregulation in CM from EPS treated myotubes to induce <i>Mmp14</i> expression. ....	61
Figure 3.8 Elevated rates of type I collagen degradation in BMDM is influenced by LIF from E(+)CM. ....	62

## LIST OF ADDITIONAL FILES

Supplementary Table 2.1 Differentially expressed genes (DEG) between 16 weeks of intervention and baseline.....	[XLSX 312 KB]
Supplementary Table 2.2 ConsensusPathdb pathway overrepresentation analysis for differentially expressed genes (DEG).....	[XLSX 27 KB]
Supplementary Table 2.3. ConsensusPathdb pathway overrepresentation analysis of differentially expressed genes (DEG) unique to metPRT.....	[XLSX 12 KB]
Supplementary Table 2.4. Young healthy muscle donors.....	[XLSX 13 KB]
Supplementary Table 2.5. List of Differentially expressed genes between young skeletal muscle and all baseline muscle old subjects.....	[XLSX 1.2 MB]
Supplementary Table 2.6. ConsensusPathdb pathway overrepresentation for genes no longer different between young and old baseline following 16 weeks common to both plaPRT and metPRT.....	[XLSX 13 KB]
Supplementary Table 2.7. ConsensusPathdb pathway overrepresentation for genes no longer different between young and old baseline following 16 weeks of metPRT only.....	[XLSX 11 KB]
Supplementary Table 3.1. Human CD11b sorted cells graph-based clustering.....	[XLSX 612 KB]
Supplementary Table 3.2. Differentially expressed genes (DEG) List Between MOV and Sham Mice.....	[XLSX 711 KB]
Supplementary Table 3.3. Differentially expressed genes (DEG) List Comparing Mmp14(+) vs Mmp14(-) macrophages.....	[XLSX 182 KB]
Supplementary Table 3.4. Differentially expressed genes comparing E(+) vs E(-) Human Primary Myotubes (FC >1.5, P <0.05).....	[XLSX 390 KB]

## **CHAPTER 1. INTRODUCTION TO SKELETAL MUSCLE MACROPHAGES AND EXTRACELLULAR MATRIX REMODELING WITH MECHANICAL OVERLOAD**

### **1.1 Skeletal muscle extracellular matrix and regulators of remodeling**

The extracellular matrix (ECM) in skeletal muscle plays an integral role in tissue development, structural support, and force transmission [1]. The ECM normally accounts for approximately 10% of muscle weight and is organized into three layers: the endomysium that surrounds individual muscle fibers, the perimysium that divides the muscle into fascicles, and the epimysium that provides external support to the entire muscle [2]. The ECM provides three fundamental functions; the first is basic mechanical support for vessels and nerves; the second is the connective tissue ensures the passive elastic response of muscle; and the third is force transmission from the muscle fibers not only to the tendon and subsequent bone via the myotendinous junctions but also via lateral transmission between neighboring fibers and fascicles within a muscle. The ECM is predominately composed of type I and III collagens, which are fibrous ECM proteins that can vary widely in content and alignment between layers and different muscle types to accommodate function [3]. Within the endomysium, these collagens converge with a specialized basement membrane that surrounds each muscle fiber. The composition of the basement membrane consists mainly of type IV collagen, laminin, and fibronectin [4]. The dystrophin associated glycoprotein provides mechanical linkage between the contractile proteins within the muscle fiber and the interconnected layers of the basement membrane and intramuscular collagens [5]. ECM turnover is a normal homeostatic process that is accelerated in response to stress or damage. When mechanical loading and strain alter muscle fiber contractile activity, size, orientations and connectivity,

remodeling processes must occur that involve both ECM deposition and degradation. ECM deposition is regulated by growth factors belonging to the transforming growth factor beta (TGF- $\beta$ ) superfamily through the phosphorylation of SMAD proteins that transduce extracellular signals to the nucleus where they activate downstream gene transcription resulting in collagen production [6]. The degradation of ECM is mediated primarily by the production of matrix metalloproteinases (MMP), cathepsins and through the cellular uptake of ECM fragments [7]. Intact fibrillar collagen can only be cleaved by a subset of MMPs (MMP1, MMP8, MMP13, and MMP14) and by other proteases, such as cathepsin K [8, 9]. Subsequently, collagen fragments can be further degraded by other members of the MMP family like MMP2 and MMP9 [10]. Transcriptomic profiling of skeletal muscle at early time points (days 3 and 7) in response to injury, mechanical loading, and reloading after periods of disuse, indicate an overrepresentation of genes related to ECM remodeling that are shared between all three stimuli [11-13]. ECM remodeling involves many cell types in muscle, but the focus of this dissertation is macrophages, which participate in the early immune response to damage and loading. Using resistance training in humans, and a surgical model of mechanical overload of mouse muscle to induce hypertrophy, the goal was to define macrophage contributions to ECM remodeling and muscle adaptation in both human and mouse skeletal muscle.

## **1.2 Macrophage characterization and activation**

In addition to the ECM remodeling gene signature, genes related to an immune response were also overexpressed at early time points in response to mechanical loading, injury and reloading following disuse [11-13]. Of the immune cells present within skeletal muscle, the most abundant immune cell type are macrophages [14]. Macrophages are

highly plastic and capable of changing their activation states in response to growth factors (e.g., CSF-1 and GM-CSF) and external cues, such as cytokines, microbes, microbial products, and other modulators, including nucleotide derivatives, antibody-Fc receptor stimulation, glucocorticoids, infection, phagocytosis, and potentially any other entity capable of being recognized by macrophages [15]. However, for many years, researchers had mainly stratified macrophages by two oversimplified classifications, derived from in vitro studies. The two classifications were termed classically activated M1 macrophages and alternatively activated M2 macrophages. Classical or alternative macrophages were produced by treating macrophage cell cultures with either interferon  $\gamma$  (M1) or interleukin-4 (M2), respectively [16]. The primary distinguishing factor between the two treatments was the elevation in pro-inflammatory cytokine expression by classical macrophages or anti-inflammatory cytokine and growth factor expression from alternative macrophages [16]. Currently, the field of skeletal muscle research more commonly identifies macrophages based on origin. The lymphocyte antigen 6C (LY6C) surface marker in mice and chemokine receptor 2 (CCR2) in humans are used to identify circulating and infiltrating monocyte-derived macrophages [17]. The axis that mediates macrophage/monocyte recruitment occurs predominantly through CCR2 and chemokine ligand 2 (CCL2) also referred to as monocyte chemoattractant protein 1 (MCP-1) [18, 19]. Resident macrophage markers include lymphatic vessel endothelial hyaluronan receptor 1 (LYVE1), mannose receptor 1 (MRC1, CD206), and scavenger receptor cysteine-rich type 1 protein M130 (CD163), which are also considered to be markers of M2 macrophages [20, 21]. Previous reports have demonstrated significant perturbations to muscle adaptations when infiltrating, as well as resident macrophages, are depleted,

however, the outcomes are generally unique to the stimulus and timepoint [22-24].

Herein we will use a similar nomenclature to describe macrophages and their contribution to skeletal muscle adaptations with an emphasis on their pro and antifibrotic roles in ECM remodeling, as well as how the muscle environment influences macrophage activation states.

### **1.3 Evidence of macrophage contribution to ECM deposition**

One of the earliest studies to demonstrate macrophage-stimulated collagen synthesis in vivo was with wound healing [25]. Macrophages isolated from the wound site, expressed transcripts for *TGF- $\beta$ 1*, platelet-derived growth factor alpha (*PDGF $\alpha$* ), and insulin-like growth factor-1 (*IGF-1*) [26]. Intriguingly, macrophages from cardiac tissue were observed to directly contribute to type IV collagen deposition [27]. Macrophages are often associated with fibrosis in chronic myopathies such Duchenne muscular dystrophy (DMD) or chronic unresolved injury, and this is thought to be largely regulated through their interactions with fibrogenic cell lineages within skeletal muscle [28]. The mechanism by which macrophages promote skeletal muscle fibrosis was eloquently described by Juban et al., who identified a mechanism where TGF- $\beta$ 1 dimerizes and complexes with latent TGF- $\beta$  binding protein (LTBP) and then interacts with the ECM [29]. These authors highlighted the necessity for adenosine monophosphate activated protein kinase (AMPK) activation to induce the expression of LTBP in macrophages [29]. AMPK has also been identified as an integral regulator of macrophage activation towards the anti-inflammatory state (see section 1.5). Fibroblasts were necessary for the activation of latent TGF- $\beta$ 1 via their secretion of a series of enzymes including bone

morphogenetic protein 1 (BMP-1) and MMP14. This complex interplay ultimately resulted in the stimulation of collagen production in fibrogenic cells [29].

#### **1.4 Evidence of macrophage contribution to ECM degradation**

Macrophages can directly affect the rate of ECM degradation by several distinct mechanisms. Skeletal muscle regeneration studies demonstrated that macrophage-derived urokinase-type plasminogen activator (PLAU) was necessary for proper injury resolution [30]. PLAU is necessary for the conversion of plasminogen into active serine proteinase, plasmin [30]. The plasminogen system is thought to play a major role in the degradation of ECM through the activation of MMPs in macrophages and other cell types present within skeletal muscle [31]. To support these findings, ECM solubilization rates were measured in macrophage cultures with and without plasminogen. The effects of plasminogen addition to the culture media resulted in a 15-fold increase in solubilization rates [32]. Several MMPs including MMP3, 8, 9, 12, 13 and 14 were reported to be expressed by macrophages in smooth muscle and cardiac muscle environments [7]. To date, MMP9 is the only MMP that has been reported to colocalize to macrophages in skeletal muscle [33]. With the vast evidence that macrophages express multiple types of MMPs in tissues outside of skeletal muscle and the advent of single cell RNA-seq (scRNA-seq), future studies aimed at identifying macrophage *MMP* expression are warranted. Targeted studies examining the consequences of macrophage-specific MMP deletion in vivo with regeneration or loading studies may uncover a fundamental aspect of macrophages that has been overlooked to date. Another mechanism by which macrophages may degrade ECM is through the phagocytosis of debris in injured and degenerating muscle [34]. Binding of collagen fragments to the cellular membrane

integrin receptor  $\alpha 2\beta 1$  results in collagen phagocytosis in macrophages in vitro [10].

Macrophage uptake of ECM in muscle has been proposed, but this mechanism of ECM degradation has never been directly tested in skeletal muscle.

### **1.5 Adverse effects of macrophage depletion on skeletal muscle adaptations following damage in mice**

Arnold et al., was the first to report that depletion of circulating monocytes at the time of injury totally prevented muscle regeneration [22]. The use of the diphtheria toxin receptor (DTR) inducible system allows for temporal deletion of cells in mice with DT injection with specificity under the control of the human ITGAM (integrin alpha M) promoter (CD11b), which is considered a pan marker of macrophages, as well as monocytes. When DT was injected simultaneously with notexin, a form of myotoxin similar to cardiotoxin, none of the hallmarks of muscle regeneration were detected, and persistence of necrotic fibers were observed out to day 7 [22]. The authors also attempted to specifically target intramuscular resident macrophages at a time point following the removal of necrotic muscle fibers. Injection of DT 7 days after notexin injection resulted in muscle fiber cross-sectional area (CSA) from the DT-injected muscle 41% smaller than control PBS-injected muscle [22], which they propose is due to the lack of myogenic differentiation of satellite cells (see below). In a follow up study, Mounier et al., identified AMPK as a major regulator of macrophage activation state during the latter regeneration periods (after day 7). Using a macrophage specific AMPK knockout mouse model, authors demonstrated that muscle fiber CSA was significantly lower 14 days after cardiotoxin injury in the knockout animals compared to wild type controls [35]. AMPK $\alpha 1$  knockout



mice also showed hindered phagocytic capacity of apoptotic cells and prolonged inflammatory signaling [35]. Additional macrophage depletion studies in mouse models of skeletal muscle regeneration using clodronate liposomes (CL), which induces apoptosis in monocytes and macrophages, corroborated the findings presented in the DTR studies [23]. Summan et al., reported similar discrepancies in the accumulation of necrotic fibers, increased fat accumulation and delays or reductions in classical early inflammatory cytokine signaling [36]. Summan et al., did not however report any differences in muscle fiber CSA at day 9 following freeze injury, but a follow up study using CL with a blunt force contusion injury, reported smaller regenerating muscle fibers at day 14 [23, 36]. In regeneration studies it is evident that macrophages play an important role in injury resolution via satellite cell activation [22]. Satellite cells, which are located beneath the basement membrane of muscle fibers, are highly influenced by macrophage soluble factors. These factors can either promote proliferative states or drive satellite cell fusion with existing muscle fibers. For instance, following cardiotoxin injury, infiltrating macrophages were shown to express cytokine C-X-C motif chemokine 10 (*CXCL10*) by scRNA-seq analysis which promoted the proliferation of satellite cells in mice [37]. In terms of satellite cell fusion, overexpression of ADAM metallopeptidase with thrombospondin type 1 motif 1 (*ADAMTS1*) in macrophages led to a greater abundance of myonuclei per fiber, presumably due to satellite cell fusion [38]. However, the significance of macrophages to muscle adaptations under mild or non-injurious models that induce muscle growth, such as resistance exercise, is less well-defined.

## **1.6 Deficits in muscle growth and regrowth with macrophage depletion in mice**

Using synergist ablation (SA), a technique where mechanical overload of the plantaris is induced by the transection of the gastrocnemius and soleus, CL treatment in mice over 14 days of overload demonstrated only a two-third increase of wet muscle weight observed in control animals [39]. Similar to muscle regeneration studies, satellite cell abundance was also significantly lower in CL treated animals compared to control animals [39]. Authors identified IGF-1 as a potential candidate for the discrepancies observed in muscle mass accrual, however, no differences were observed in the phosphorylation of mechanistic target of rapamycin complex 1 (mTORC1), a known downstream target of IGF-1, in skeletal muscle [39]. This observation is of particular interest when relating hypertrophy to regeneration studies due to previous reports that macrophage specific deletion of IGF-1 resulted in smaller muscle fibers following cardiotoxin induced injury [40].

Hindlimb muscle unloading for 10 days followed by reloading for 4 days is a model to induce dynamic changes in muscle fiber CSA, that are associated with a robust immune response [41]. Tidball et al., used this model in combination with intraperitoneal injections of anti-F4/80, which binds a mouse macrophage surface antigen and results in their apoptosis, to identify whether macrophages play a role in regrowth and tissue repair. Effective depletion was observed at day 4 which coincided with a significantly smaller muscle fiber CSA compared to control animals in the soleus [42]. The authors also showed a greater proportion of fibers with membrane damage at day 4 in the macrophage depleted animals [42]. Recently, a publication described a mechanism by which resident macrophages may cloak tissue microlesions to prevent neutrophil-driven inflammatory

damage [43]. It is likely that models of reloading, as well as synergist ablation, induce microlesions following the onset of loading and macrophages may play an important role in preventing excess tissue damage and preserve tissue homeostasis.

### **1.7 Macrophages in human skeletal muscle adaptation**

Compared to studies of macrophages in response to rodent injury and loading, relatively few studies have attempted to understand the role of macrophages in human muscle adaptation to injury or exercise [44-47]. Mackey et al., used forced lengthening contractions induced by electrical stimulation to produce muscle fiber injury in young healthy males. Immuno-stained single muscle fibers revealed a repeating pattern of necrotic and regenerating zones along the length of the same muscle characterized by extensive macrophage infiltration alongside differentiating myogenic progenitor cells and myotubes. We have consistently demonstrated a significant increase in macrophage abundance following exercise training in middle aged and older adults on skeletal muscle cross-sections using antibodies against both CD11b and CD206 markers [44, 48]. Walton et al., found several interesting associations between the change in macrophage abundance and changes in muscle fiber CSA, as well satellite cell abundance, following 12-weeks of cycle training in a cohort of healthy middle-aged adults [44]. Walton et al., also identified several ECM related genes (*MMP14*, *SERPINE1*, *SPARC*, *ELN*, *COL5A1*, *COL6A1*, *TGFB1* and *LOX*) that were all positively and significantly associated with changes in macrophage abundance following 12-weeks of training. In a recent publication, Jensen et al., reported a significant increase in macrophage accumulation and type I collagen expression at day 4 and 7 in healthy older male adults following an acute bout of resistance exercise [47]. Macrophages appear to be an important facilitator of

skeletal muscle ‘growth and we propose to test the hypothesis that ECM remodeling is an important underlying mechanism.

## **1.8 Skeletal muscle influence on macrophage activation state**

Studies both in vivo and in vitro have demonstrated that macrophages can undergo dynamic transitions in activation states [29, 34, 49]. Recently, different regulatory pathways have been associated with macrophage activation states and involve a variety of molecular mechanisms at the genomic, transcriptomic, and post-transcriptomic levels (reviewed in [50]). Despite these recent advances, the signaling pathways responsive to muscle contraction that regulate macrophage activation state remains poorly understood. One recent study was able to gain insight into this interaction by using a muscle specific overexpression model in mice and cells in vitro. The overexpression of peroxisome proliferation activator receptor- $\gamma$  (PPAR- $\gamma$ ) coactivator -1 $\alpha$  (PGC-1 $\alpha$ ), which is elevated following exercise, induced the release of secretion phosphoprotein 1 (SPP1) which promoted an increase in macrophage abundance. In vitro studies demonstrated SPP1 strongly upregulated *MCP-1* expression in macrophages, which influenced the recruitment of other mononuclear cells such as endothelial cells that also express *CCR2* [51]. A primary objective of this dissertation is to contribute to this body of literature by identifying other novel pathways that may alter macrophage activation state to promote muscle adaptation in response to hypertrophic stimuli.

## **1.9 Preview of studies presented**

In Chapter 2, we performed bulk RNA-sequencing of human skeletal muscle from healthy older adults before and after 14-weeks of progressive resistance exercise training

(PRT) with and without the AMPK agonist, metformin. We hypothesized that AMPK activation would promote a greater increase in the anti-inflammatory activation states of macrophages, and in turn create an environment more conducive for skeletal muscle growth in older adults with PRT. Although metformin had no effect on macrophage activation state, PRT significantly increased macrophage abundance in both placebo and metformin treated groups [48]. ECM remodeling was the most overrepresented pathway in response to PRT regardless of treatment group, which led to a mechanistic exploration of macrophage function in relation to ECM remodeling in Chapter 3. We were able to identify a candidate gene, *MMP14*, that was increased following PRT, previously shown to positively correlate to the change in macrophage abundance with exercise [44], and potential molecular pathways regulating *MMP14* expression. We used several different in vivo and in vitro models to explore mechanisms whereby contracting muscle releases soluble factors that promote macrophage-mediated ECM degradation. Chapter 4 highlights the novelty of our findings with a focus on the understudied crosstalk between skeletal muscle fibers and macrophages in response to hypertrophic stimuli. This information will aid future researchers who are keen on targeting macrophages to promote ECM remodeling and improve skeletal muscle adaptations.

## CHAPTER 2. METFORMIN ALTERS SKELETAL MUSCLE TRANSCRIPTOME ADAPTATIONS TO RESISTANCE TRAINING IN OLDER ADULTS

### 2.1 Introduction

Biological aging is characterized by a progressive decline of physiological and metabolic functions across multiple organ systems. One of the key phenotypes of aging is the loss of skeletal muscle mass, a condition known as age-associated muscle atrophy or sarcopenia [52-54]. This is usually accompanied by reduced strength, muscle quality and mobility, increased risk of frailty and falls, lack of endurance and poor physical performance [55]. In the western population, >40% of adults over the age of 60 have difficulties with daily activities such as walking or standing up from a chair etc. and >30% suffer from some kind of physical disability [56]. After the age of 60, striking changes occur in muscle physiology, corresponding to a decline in muscle mass and deterioration of muscle strength by ~2% each year [57]. The pathophysiology of age-related decline in muscle mass and function is multifactorial, including biological factors such as hormonal imbalance, neurodegeneration and motor neuron loss, increased inflammation and circulating cytokines, as well as environmental factors such as physical inactivity, inadequate nutritional intake and psychosocial factors [55, 56, 58]. Furthermore, age-associated changes in muscle metabolism, such as mitochondrial dysfunction and insulin resistance, can have severe implications in muscle homeostasis and regeneration [59, 60]. We have shown that progressive resistance exercise training (PRT) induces meaningful increases in muscle strength, power, and functional mobility, however, the hypertrophic response is, on average, reduced in old compared to young,

especially within men [61]. The hypertrophic response to PRT is also highly variable in older adults (reviewed in [62]).

The use of pharmacological interventions to augment the effect of PRT on muscle hypertrophy in the older adults has been proposed [63-66]. The biguanide metformin has been studied in the context of exercise capacity, quality of life and mood states, and metabolic adaptations, such as insulin production and clearance, oxidative stress and cardiometabolic health in older adults with prediabetes and Type II diabetes [67-69]. Metformin has been extensively used since the 1950s, as the first-line treatment against Type II diabetes and is one of the most commonly prescribed drugs in the world, either as a monotherapy or in combination with insulin or other anti-hyperglycemic agents [70]. Metformin directly inhibits mitochondrial enzymes including Complex I [71], activates AMP-activated protein kinase (AMPK) [72], inhibits NF- $\kappa$ B signaling and specifically blunts the secretion of proinflammatory cytokines in macrophages [73, 74]. Due to its role beyond anti-hyperglycemia in modulating several fundamental pathways disrupted during chronic diseases and aging, repurposing metformin to treat cardiovascular diseases, cognitive decline, cancers, neurodegenerative diseases and ultimately, aging as a whole, has been proposed [75-80].

Two studies have shown that short-term metformin treatment and exercise do not exhibit synergy, but work in an antagonistic manner, where metformin attenuates the insulin sensitizing effect of exercise [81, 82]. Metformin has been shown to induce

physiologically subtle decreases in peak aerobic capacity evidenced by a reduction in peak oxygen uptake, peak heart rate, peak ventilation, peak respiratory exchange ratio and exercise duration [83]. However, another study in prediabetic adults concluded that metformin in combination with aerobic and resistance exercise training lowered proinsulin concentrations and increased insulin clearance [84]. Recently, Konopka et al showed in older adults that metformin blunted aerobic exercise training-induced improvements in cardiorespiratory fitness, insulin sensitivity, and prevented the gain in muscle mitochondrial respiration capacity [85]. Thus, there may be a complex interplay between molecular mechanisms of exercise adaptations and pathways affected by metformin.

We originally undertook the MASTERS Trial to test the hypothesis that metformin would act synergistically with PRT to reduce the number of exercise non-responders regularly observed among older adults by reducing muscle inflammation. However, in the MASTERS Trial, metformin plus PRT inhibited muscle growth after 14 weeks of training [48]. In vitro, acute metformin treatment of human primary myotubes undergoing electrical pulse stimulation (exercise mimetic capable of inducing myotube hypertrophy) had a repressive effect on mTORC1 signaling, and upregulated AMPK phosphorylation [48]. Thus, metformin's impairment of cardiorespiratory fitness and muscle mass gains in physically active older adults must be reconciled with benefits associated with health span.



The purpose of this study was to map the muscle transcriptional response to PRT with or without adjunctive metformin in the MASTERS Trial, to identify potential mechanisms contributing to the blunted hypertrophic response in older adults [48]. Previously, global gene expression studies of human skeletal muscle aging have identified mitochondrial dysfunction, extracellular matrix organization, complement activation and ribosomal pathways comprising a differentially expressed aging signature [86, 87]. Effects of PRT on this signature, with and without metformin, may identify new intervention targets that counteract sarcopenia, and provide information on potential metformin-exercise interactions in muscle that are relevant to repurposing metformin to treat aging and age-related disorders.

## **2.2 Methods**

### **2.2.1 Study Design, Participants and Interventions**

The Metformin to Augment Strength Training Effective Response in Seniors (MASTERS) Trial is a randomized, controlled, double blind trial comparing the effects of metformin versus placebo during a 14-week progressive resistance exercise training (PRT) intervention in healthy men and women  $\geq 65$  years of age. Participants were recruited at University of Kentucky and University of Alabama at Birmingham, UAB. The detailed study design [88] and participant characteristics [48] have been published previously.

Participants were randomized to receive either placebo or metformin for the duration of the trial. Subjects underwent a two-week drug or placebo wash-in period prior to beginning PRT. Those who were randomized to metformin were titrated up to the target

dose by taking 1 tablet per day (850 mg) for 7 days, followed by 2 tablets per day (1700 mg) for the remainder of the trial.

All study subjects underwent 14 weeks of PRT, supervised by trained personnel. We employed a variable intensity prescription across the three training days each week (high/low/high) based on the results of our previous dose-response trial which showed this prescription optimized strength and muscle mass gains in older adults [89]. Vastus lateralis muscle biopsies were obtained prior to drug initiation and 3 days after the final bout of training. Primary outcomes of the trial, muscle size and strength, have been reported [48]. Vastus lateralis muscle biopsies from young individuals matched for body mass index were obtained through the Center for Muscle Biology at the University of Kentucky.

### **2.2.2 Library Preparation**

Total RNA was isolated from baseline muscle biopsies in 37 plaPRT and 28 metPRT participants and from 14-week post-training muscle biopsies in 26 plaPRT and 24 metPRT participants (average age 71 years old). Of these, 24 plaPRT and 23 metPRT participants had biopsies at both timepoints. Additionally, total RNA was isolated from muscle biopsies in 21 young healthy donors (average age 24 years old). Approximately 35 mg of muscle was subjected to bead homogenization in Qiazol (Qiagen, Valencia, CA) and RNA purified using miRNeasy Mini Kits (Qiagen) and stored at -80°C. RNA content, integrity and purity were determined with a Nanodrop 2000 spectrophotometer (Thermo Fisher, Waltham, MA) and the 2100 Bioanalyzer (Agilent, Santa Clara, CA). A minimum RNA Integrity Number (RIN) of 6.5 was set for all samples.

### 2.2.3 Sequencing, Preprocessing and Alignment

Total RNA was sequenced at Novogene Corporation, Chula Vista, CA on an Illumina HiSeq 4000 system, using a standard paired-end 150 bp (PE150) dual indexing protocol. The two sets of samples (University of Kentucky and University of Alabama), each containing samples from all timepoints of both placebo and metformin arm as well as young, were sequenced in different batches that were corrected for in the downstream analyses. Raw fastq sequence reads were passed through quality control using FastQC (0.11.4) [90] and the QC results were compiled for all samples using MultiQC (1.7) [91]. Due to adapter contamination, the raw fastq files were trimmed for adapter sequences, filtered for low quality reads and too short reads, using the default parameters in *fastp* (0.19.4) - an all-in-one preprocessing tool for fastq files [92]. After checking for QC using the same steps as before, RNA-Sequencing by Expectation Maximization- RSEM (1.3.0) in conjunction with the STAR aligner (2.6.1b) was used to align the raw reads to the GRCh38 primary assembly build of the reference human genome, with transcript annotations (gencode.v29.annotation.gtf) downloaded from GENCODE [93-95].

### 2.2.4 Differential Gene Expression Analysis

All statistical analysis for the gene expression data were carried out using the R statistical software (R-3.6.0). The raw counts were filtered for low expression using a counts-per-million (cpm) threshold of 0.6 (10/minimum library size) in at least 24 (number of samples in the smallest group of comparison). Since the principal component analyses revealed a distinct sequencing batch effect, the raw count data was corrected for it using *batch* as a covariate in the generalized linear model in limma (3.4.0) [96]. The corrected

data using the *removeBatchEffect* function in limma was deemed to have minimal sequencing batch effects after a visual inspection of PCA and used for all downstream analyses. Raw data were normalized using the trimmed mean of M-values (TMM) normalization. To minimize heteroscedasticity from the count data and incorporate precision weights to account for the mean-variance relationship, the *voom* function was applied on the normalized data [96]. A linear model was fit on the voom-normalized data, while adjusting for the study arm (placebo vs metformin) and biopsy time (baseline, 14-weeks of PRT with treatment and young). Due to the paired nature of the study, the participant id was used as a blocking variable. Differential gene expression was measured using an Empirical Bayes statistic in limma for the following comparisons; plaPRT vs Baseline, metPRT vs Baseline, Young vs Old Baseline, Young vs plaPRT (14 weeks), and Young vs metPRT (14 weeks). The raw P-values were adjusted for multiple comparisons using the Benjamini-Hochberg correction. The adjusted P-value threshold of 0.01 was used to characterize statistically significant differentially expressed genes (DEG).

### **2.2.5 Pathway Overrepresentation Analysis**

Genes that were deemed to be differentially expressed with statistical significance (Adj-P <0.01), were exported to ConsensusPathdb (<http://cpdb.molgen.mpg.de/CPDB>) database [97]. The pathways interrogated were Reactome, KEGG, Biocarta, Wikipathways and PharmGKB. A hypergeometric test was run and pathways with a gene overlap threshold of 10% of all input genes and the p-value cutoff of 0.01 were included in the output. Duplicated pathways were excluded from the output.

### **2.2.6 Data availability statement**

The raw RNA-Seq and count data from this experiment will be accessible in the Gene Expression Omnibus database (GEO Accession code- GSE157585).

## **2.3 Results**

### **2.3.1 Global gene expression changes in skeletal muscle with placebo + progressive resistance training (plaPRT) or metformin + progressive resistance training (metPRT)**

Research participants were randomized in a double-blind fashion to placebo or metformin for 2 weeks followed by 14 weeks of PRT with continued drug treatment. Vastus lateralis biopsies were obtained at baseline (prior to drug treatment) and at 16 weeks (following 14-weeks of training) [48]. Fourteen weeks of placebo plus PRT (plaPRT) induced differential expression of 2048 genes (Adj-P <0.01), with 1161 genes upregulated and 887 downregulated (Figure 2.1A). The combination of metformin and PRT (metPRT) resulted in differential expression of 1435 genes (Adj-P <0.01), with 817 genes upregulated and 618 downregulated compared to baseline (Figure 2.1B). Principal component analysis (PCA) demonstrated a clear effect of PRT with a similar shift in the global gene expression profiles in both treatment groups (Figure 2.1C), with the Venn diagram illustrating an overlap of 918 genes (Figure 2.1D). The correlation between fold changes of the 918 common genes between the two groups was 0.97 ( $P=2.2e-16$ ), with no genes showing any anticorrelation (Figure 2.1E). Eleven hundred thirty genes were exclusively altered in plaPRT, while 517 genes were changed only in metPRT. Gene lists are included in Supplementary Table 2.1. We found no significant change in

inflammatory pathway gene expression with either plaPRT or metPRT, which argues against our original hypothesis that metformin and PRT reduce muscle inflammation.

### **2.3.2 Pathway overrepresentation within differentially expressed genes (DEG)**

Both interventions modulated transcripts involved in anabolic cell signaling, extracellular matrix (ECM) organization, and RNA metabolism pathways, suggesting a conservation of these processes in response to PRT with metformin. The directionality of changes in gene expression demonstrate that ECM genes including collagen genes (*COL1A1*, *COL3A1*, *COL4A1*, *COL6A2* etc.), ECM-receptor interaction genes, focal adhesion genes, and those encoding matrix metalloproteinases (*MMP2*, *MMP11*, *MMP14*) and laminin subunits were upregulated in both groups in response to training. On the other hand, genes belonging to mRNA splicing, RNA metabolism and post-transcriptional processing pathways were mostly downregulated. These included several nuclear ribonucleoproteins, serine and arginine rich splicing factors, RNA polymerase II subunit C, as well as pre-mRNA processing factors (Figures 2.2A and B, Supplementary Table 2.2). However, the number of DEG was higher for all pathways in plaPRT than metPRT (Figure 2.2C).

Of the 517 genes that changed exclusively in the metPRT group, pathway analysis illustrated an overrepresentation of aging hallmarks including cellular senescence, and autophagy [98], as well as post-translational modification pathways, specifically neddylation and ubiquitination (Figure 2.2D, Supplementary Table 2.3). Our previous work with short-term metformin treatment alone showed improvement in aging-induced pathways through inhibition of mTORC1 regulated genes in skeletal muscle of older

adults [99]; however, it is unclear how changes in gene expression observed here in metPRT might alter the older adult muscle phenotype.

### **2.3.3 Reversal of the aging skeletal muscle transcriptome with PRT and metformin**

In lieu of our findings that metPRT appeared to affect pathways associated with aging, we performed RNA-sequencing on skeletal muscle biopsies from 21 young individuals (mean age 24, 11 females, 10 males, Supplementary Table 2.4) under resting conditions and compared their transcriptome to that of week 0 baseline biopsies from the older adult trial participants. Our analysis revealed that 4654 DEG were present when comparing baseline biopsies ( $\text{Adj-P} < 0.01$ ) with 2446 upregulated and 2208 downregulated (Figure 2.3A, Supplementary Table 2.5). Following 14 weeks of PRT, the week 16 time point from plaPRT compared to young demonstrated a dramatic decrease in DEG that were previously observed at baseline (2898 DEG), with 1089 new DEG apparent following 14 weeks of plaPRT (Figure 2.3B, Supplementary Table 2.5). MetPRT further reduced the number of DEG compared to young muscle to 2705, however, the number of unique DEG that were present after 14-weeks of PRT was also lower compared to placebo (837 DEG), which is consistent with our initial findings that metformin blunts the overall transcriptomic response to PRT (Figure 2.3B, Supplementary Table 2.5). Young vs old baseline DEG that were lost following PRT in both groups (1483) include RNA splicing and numerous genes involved in longevity-associated pathways (Figure 2.3C, Supplementary Table 2.6). After identifying DEG between young and old muscle at baseline that were no longer differentially expressed at week 16 in both plaPRT and metPRT, we identified 466 DEG that returned to young expression levels only in

metPRT. Pathway overrepresentation analysis showed that these genes were largely involved in metabolism, particularly lipid metabolism (Supplementary Table 2.7).

## **2.4 Discussion**

In this study, we characterized the effect of metformin on the skeletal muscle transcriptomic response to PRT in older individuals from the MASTERS Trial [48]. Our results indicate that PRT induces substantial transcriptional changes in skeletal muscle with upregulation of genes involved in extracellular matrix (ECM) remodeling and downregulation of mRNA processing genes being the most affected. We also provide evidence that metformin reduces skeletal muscle adaptations to PRT at the transcriptomic level, consistent with the decreases in physiological gains in response to PRT in lean body mass, and thigh muscle mass and area, as we have previously reported in this cohort [48]. Recently, the complex interaction between metformin and aerobic exercise training was described, showing that metformin also blunts improvements in physiological functions and mitochondrial adaptations otherwise promoted by aerobic exercise training in older adults [85]. Similarly, the present findings suggest that key molecular cues underlying adaptations to PRT are attenuated by metformin. Nevertheless, we discovered gene sets differentially regulated by the combination of PRT and metformin that may promote health benefits separate from PRT-induced muscle hypertrophy.

Skeletal muscle ECM is crucial to force transmission, structural integrity and muscle stem cell dynamics [4, 100], and ECM remodeling is hypothesized to be critical for muscle fiber growth [101]. A large number of genes associated with pathways involved



in ECM composition and reorganization were upregulated in both plaPRT and metPRT groups, but to a lesser magnitude in metPRT, potentially contributing to the reduced growth response. Resistance exercise training in middle aged adults has been shown to upregulate collagens and MMPs [102]. In particular, MMP2 has been shown to be necessary for skeletal muscle hypertrophy [103]. We found significant up-regulation of MMP2 mRNA in response to PRT in both groups, suggesting that metformin may not interfere with this specific effect of PRT that may contribute to muscle remodeling.

Genes belonging to mRNA splicing and post-transcriptional processing pathways were mostly downregulated in both groups. Aging is accompanied by a dysregulation in the splicing machinery including a rise in splicing factors, especially the heterogeneous nuclear ribonucleoproteins (hnRNPs) [104, 105]. We observed a systematic suppression of multiple hnRNPs and mRNAs encoding RNA processing and splicing factors, with down regulation of RNA processing pathways more prominent in plaPRT. Several studies have demonstrated that alternative splicing is highly enriched in energetically demanding tissues such as muscle and brain [106]. Upregulation of alternative splicing in skeletal muscle with aging may activate damage-response mechanisms at a time when energy becomes scarce [105]. Physical activity in older adults was shown to offset the changes in splicing machinery [107] and although the functional relevance has yet to be established, this effect may reduce the number of genes that are differentially spliced and the number of splicing errors that produce non-functional proteins that tend to increase with age [108].

To our knowledge only one other study has performed transcriptome analysis using microarrays to compare the effects of PRT in healthy older subjects to that of young resting skeletal muscle [109]. This seminal study illustrated that 596 genes were differentially expressed at baseline between young and old. Following 6 months of resistance exercise training a total of 179 of the 596 were no longer significantly different to that of young. Although our DEG lists are much larger, which is likely due to the greater number of older subjects at baseline between studies (65 vs 25), as well as our end point (50 vs 14), we did find commonalities between gene lists including cell cycle inhibitors *p21* and *p15*, as well as many metabolism related genes. Melov S et al. gene ontology analysis demonstrated that metabolic and mitochondrial function were largely impacted by aging and that resistance exercise training had a significant effect on reversing these age-related deficits [109]. Presently, we observed a similar response with PRT in both cohorts; however, adjunctive metformin further reduced the number of DEG between young and old, which appeared largely due to metformin's effects on genes related to metabolism; pathway overrepresentation indicated a return to young gene expression patterns related to lipid metabolism preferentially in metPRT. In our primary findings of the trial, we reported an increase in AMPK/ACC phosphorylation in metPRT, that may affect lipogenesis [48]. The known inhibition of Complex I by metformin [71] coupled with the increased energy demand of PRT may have led to compensatory activation of pathways involved in lipid metabolism that were previously dysregulated with age at baseline. However, it should be noted that outcomes from the MASTERS Trial showed that the PRT-induced decreases in low density muscle (which contains more intramyocellular lipid than normal density muscle) was similar between

groups, whereas plaPRT gained significantly more normal density muscle area than metPRT [48]. Thus, the combined effects of metformin and exercise on muscle density and lipid content require further study.

A few limitations reduce the scope of our interpretation of the data, including the time between the last bout of exercise and tissue collection (3 days). It is possible that metformin inhibited mTOR signaling acutely after each exercise bout, impairing growth, but did not affect the new homeostasis following training. Although we reported down-regulation of mTOR-associated pathways in muscle following 6 weeks of metformin alone in a crossover study design in older adults [110], chronic effects of metformin on mTOR regulated pathways were less apparent within the context of exercise training. Another limitation acknowledged in our primary outcomes paper is the lack of a sedentary control group given metformin for 16 weeks. We attempted to extrapolate metformin-specific effects, but without a sedentary group, it is not possible to assess effects due to metformin or the combined effects of PRT + metformin on gene expression.

In conclusion, the blunted transcriptomic response to PRT in the presence of metformin is consistent with the blunted muscle hypertrophic growth response reported in the primary outcome of the MASTERS Trial [48]. However, specific effects of adjunctive metformin on the muscle transcriptomic response to PRT, separate from those related to muscle remodeling, may alter age-associated deficits in muscle metabolism to improve function.

Metformin and PRT have beneficial effects on health that extend well-beyond skeletal muscle that should be considered. However, a metformin-exercise interaction in muscle must be defined in more detail to better inform whether metformin for healthy, physically active older adults is a correct choice.

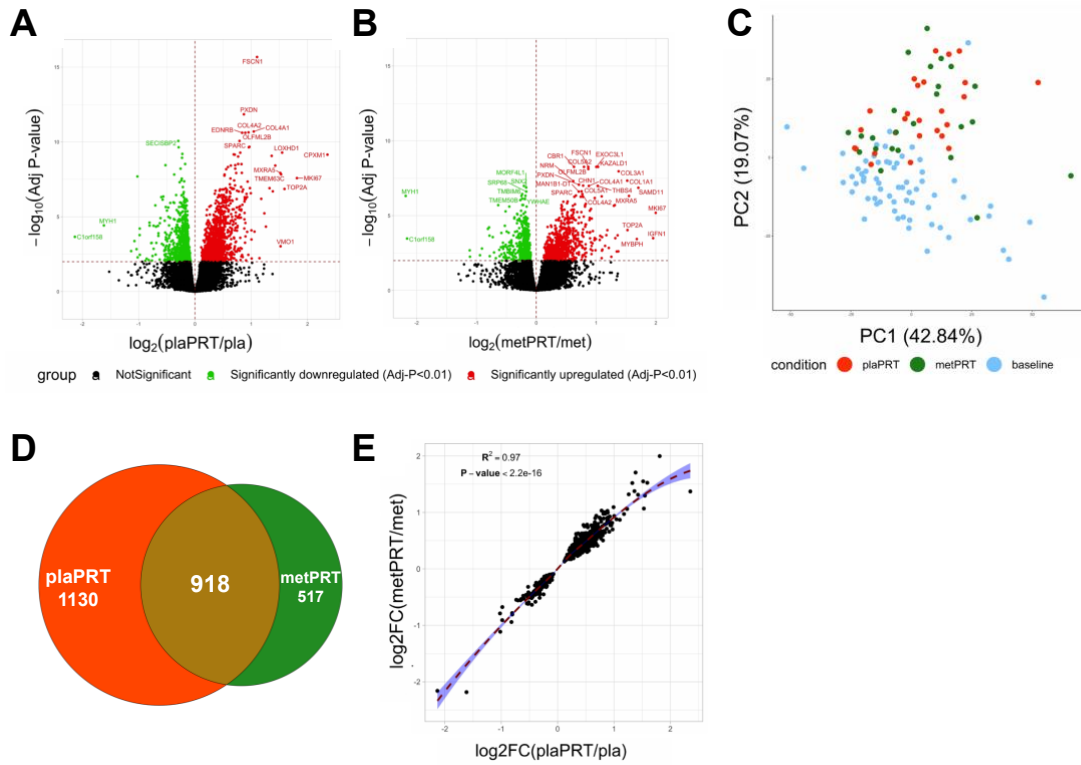


Figure 2.1 Metformin blunts the global transcriptomic changes induced by PRT in human skeletal muscle. A) Volcano plot of 2048 DEG (Adj-P < 0.01) with plaPRT between 16 weeks and baseline; B) Volcano plot of 1435 DEG (Adj-P < 0.01) with metPRT intervention between 16 weeks and baseline; C) Principal component analysis on DEG shared between plaPRT (orange) and metPRT (green) compared to baseline (blue); D) Venn diagram showing an overlap of DEG common between plaPRT and metPRT vs baseline; E) Correlation plot between the fold changes of DEG common between plaPRT and metPRT. DEG, differentially expressed genes; PRT, progressive resistance exercise training. N=23 metPRT and 24 plaPRT. DEG, differentially expressed genes; PRT, progressive resistance exercise training.

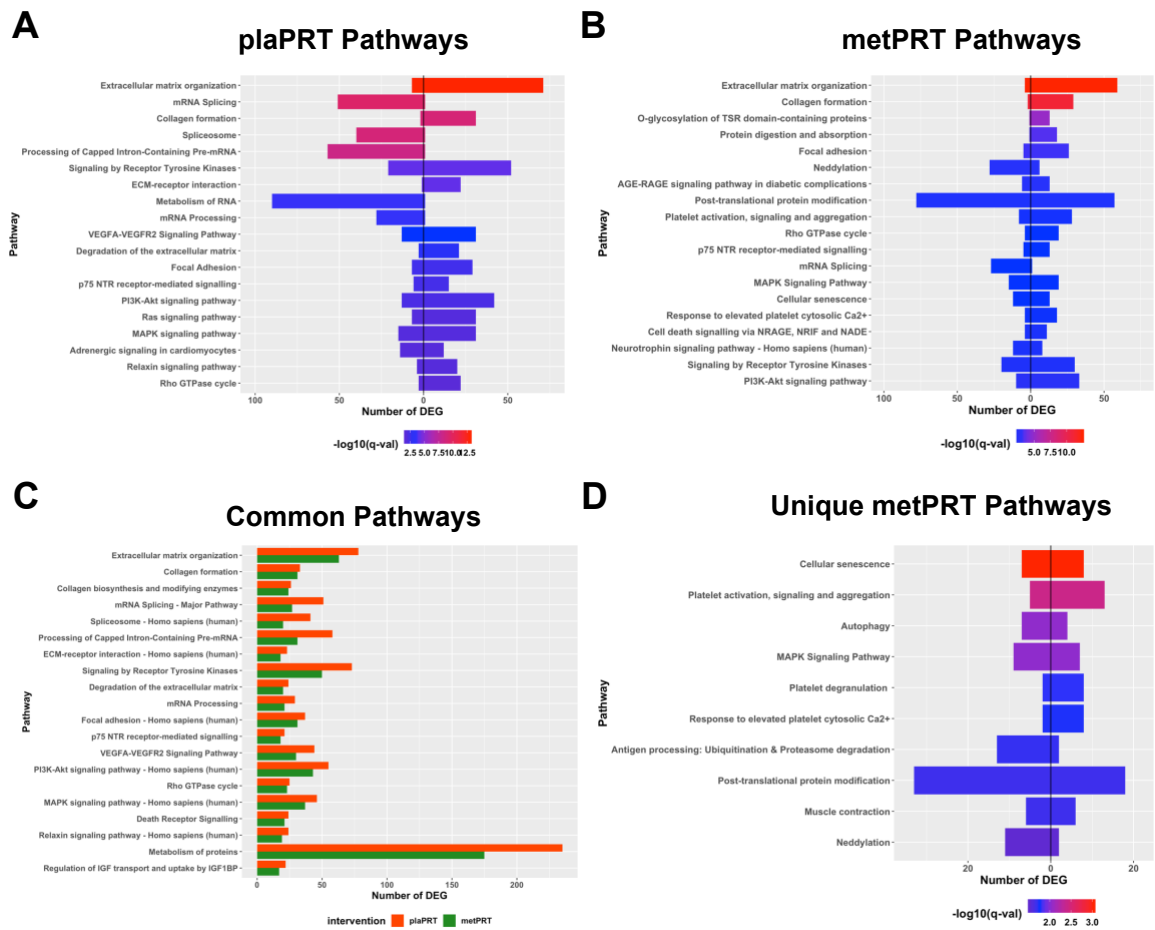


Figure 2.2 Pathway overrepresentation analyses on differentially expressed genes (DEG). A) Pathways overrepresented in plaPRT-induced DEG with the length of the bar representing the number of DEG (upregulated genes to the right and downregulated genes to the left); B) Pathways overrepresented in metPRT-induced DEG; C) Common pathways overrepresented between the plaPRT (orange) and metPRT (green) groups; D) Pathways overrepresented in the 517 DEG within the metPRT group that do not overlap with the DEG for the plaPRT group. DEG, differentially expressed genes; PRT, progressive resistance exercise training.

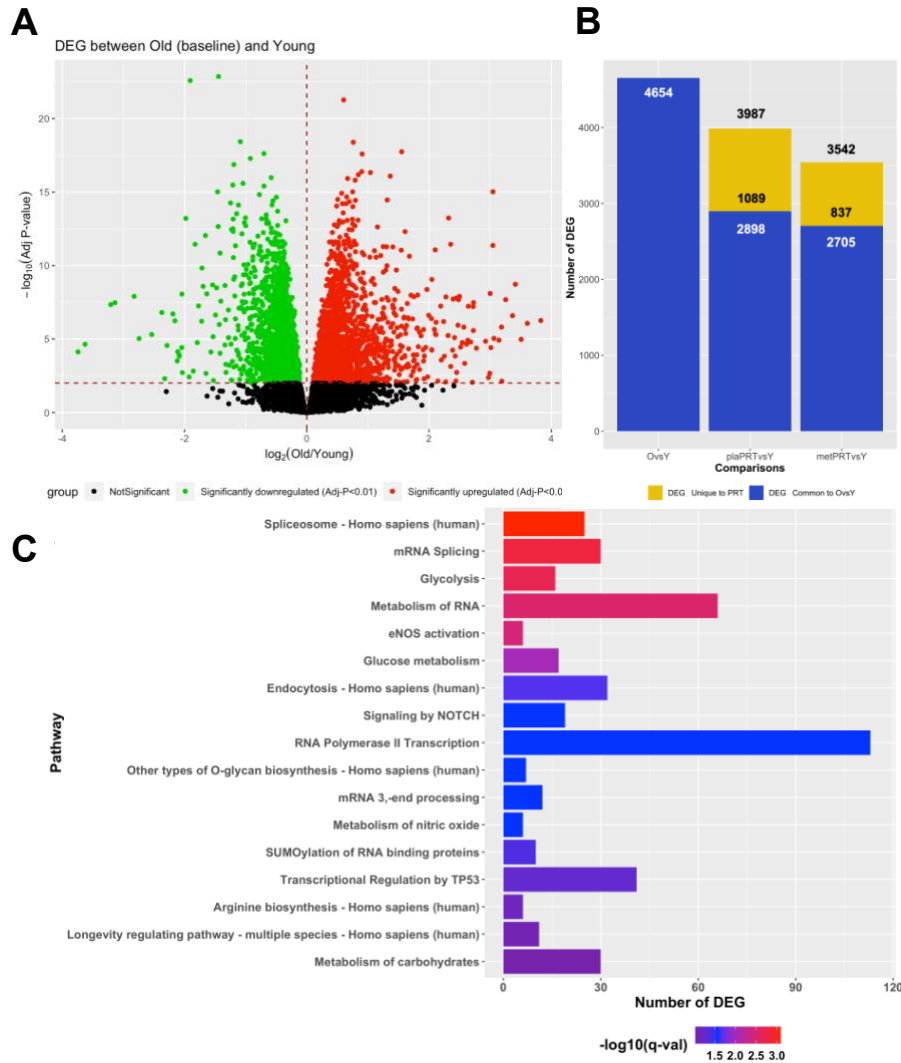


Figure 2.3 PRT reverts aging transcriptome towards that of young resting muscle and the effects of metformin are additive. A) Volcano plot of 4654 DEG (Adj-P <0.01) between young and old muscle at baseline; B) Number of DEG observed when comparing young baseline skeletal muscle to old baseline skeletal muscle (4654 DEG) and young baseline to old 16 weeks with either plaPRT (3987 DEG) or metPRT (3542 DEG). Dark blue represents DEG common to throughout all time points and yellow represents those unique to week 16 time point in either plaPRT or metPRT; C) Pathways overrepresented from those genes common to both groups following 14-weeks of PRT that were no different from young. DEG, differentially expressed genes; PRT, progressive resistance exercise training.

## CHAPTER 3. MACROPHAGE CONTRIBUTION TO EXTRACELLULAR MATRIX REMODELING WITH MECHANICAL OVERLOAD

### 3.1 Introduction

The extracellular matrix (ECM) in skeletal muscle plays an integral role in tissue development, structural support, and force transmission [1]. The ECM normally accounts for approximately 10% of muscle weight and is organized into three layers (epimysium, perimysium and endomysium) [2]. The ECM is dominated by type I and III collagens, which are fibrous ECM proteins that can vary widely in content and alignment between layers and different muscle types to accommodate function. Within the endomysium, these collagens converge with a specialized basement membrane that surrounds each muscle fiber. The composition of the basement membrane consists mainly of type IV collagen, laminin, and fibronectin. Upon mechanical loading and strain, which alter muscle fiber contractile activity, size, orientation and connectivity, remodeling processes must occur that involve both ECM deposition and degradation [3]. The degradation of ECM is mediated primarily by the production of matrix metalloproteinases (MMP), cathepsins and through the cellular uptake of ECM fragments. Intact fibrillar collagen can only be cleaved by a subset of MMPs (MMP1, MMP8, MMP13, and MMP14) and by other proteases, such as cathepsin K [8, 9]. Subsequently, collagen fragments can be further degraded by other members of the MMP family such as MMP2 and MMP9 [10]. Transcriptomic profiling of skeletal muscle at early time points (days 3 and 7) in response to injury, mechanical overload, and reloading after periods of disuse, indicate an overrepresentation of genes related to ECM remodeling that is shared between all three stimuli [11-13]. ECM remodeling involves many cell types in muscle, but the focus of



our research was directed towards macrophages, which participate in the early immune response to tissue damage and mechanical loading. Using resistance training in humans, and a surgical model of muscle mechanical overload (MOV) in mouse to induce hypertrophy, the goal was to define macrophage contributions to ECM remodeling and muscle adaptations.

We have consistently demonstrated a significant increase in skeletal muscle macrophage abundance using pan markers (CD11b/CD68) and anti-inflammatory markers (CD206/CD163) following exercise training in both middle-aged and older adults [44, 48]. Walton et al., also identified several ECM related genes (*MMP14*, *SERPINE1*, *SPARC*, *ELN*, *COL5A1*, *COL6A1*, *TGFB1* and *LOX*) that were all positively and significantly associated with changes in macrophage abundance following 12-weeks of cycle training [44]. We recently reported that with 14-weeks of progressive resistance exercise training (PRT) in older adults (>65 years of age), genes involved in ECM remodeling, including *MMP14*, were the most upregulated, differentially expressed genes among those identified by RNA-seq [137]. *MMP14* is a potent membrane-tethered collagenase that can cleave type I collagen and is also capable of activating other MMPs (*MMP2* and *MMP9*) from their latent pro-MMP complex [111]. Although very little evidence exists in terms of macrophage-specific MMP-mediated ECM remodeling during skeletal muscle regeneration or exercise training, macrophage-derived urokinase-type plasminogen activator (PLAU), which is an upstream activator of all MMPs, has been reported to play a significant role in injury resolution following skeletal muscle injury [112]. In terms of muscle-macrophage crosstalk, we also sought to identify potential

secretory factors that may alter macrophage function, beyond recruitment, and may influence *MMP14* expression in macrophages.

Upstream regulators of *MMP14* expression include the leukemia inhibitory factor (LIF) and interleukin 6 (IL6) family of cytokines, a process that was first discovered in human colorectal cancer cells [113]. LIF is a closely related cousin to IL6 and both display a similar signaling network that involves the targeted degradation of tumor protein p53 (p53), a known repressor of *MMP14* expression [113]. LIF/IL6 function by binding to the gp130-janus associated kinase (JAK) receptor and stimulating phosphorylation of STAT3 [114]. Phosphorylated STAT3 then translocates to the nucleus where it transcriptionally induces inhibitor of DNA-binding 1 (ID1). ID1 upregulates the expression of E3 ubiquitin ligase mouse double minute 2 homolog (MDM2), whose key target is p53 [114]. The degradation of p53 enables specificity protein 1 (Sp1) transcription factor to access the promoter region of *MMP14* that was previously blocked by p53 and promote transcription of *MMP14* gene. We hypothesize that MOV induces the expression of *LIF/IL6* from skeletal muscle fibers, which drives *MMP14* expression in resident macrophages and promotes the degradation of type I collagen. We used several different in vivo and in vitro models to test this hypothesis. Findings from these studies highlight a novel and understudied crosstalk between skeletal muscle fibers and macrophages with MOV that may be important for ECM remodeling to promote hypertrophy.

## **3.2 Methods**

### **3.2.1 Human subjects and intervention**

Data were acquired from the MASTERS trial (NCT02308228), which was conducted to determine whether metformin could augment the response to 14-weeks of PRT in healthy older adults, age > 65 years old. Full details of the study protocol, including participant inclusion/exclusion criteria and the PRT paradigm designed to optimize muscle mass and strength gains, can be found elsewhere [88]. The trial was conducted at the University of Kentucky and the University of Alabama at Birmingham, and all participants signed an informed consent approved by university IRBs prior to study enrollment. 24 participants from the placebo only group completed the exercise intervention and were included in this analysis. Muscle biopsies from the vastus lateralis were collected two weeks before the 14-week PRT program began and then a final biopsy 3 days after their last bout of exercise.

One participant, age 87 years old, from the placebo group in the MASTERS trial who responded well to 14-weeks of PRT was recruited for an acute bout of exercise for single cell RNA-sequencing (scRNA-seq) analysis. The subject was required to provide a muscle biopsy from the vastus lateralis 24 hours after one session of unilateral knee extension resistance exercise. Briefly, the subject performed 5 sets of 10 concentric repetitions at 70% 1 rep maximum.

### **3.2.2 Muscle Biopsies**

For all MASTERS participants, muscle biopsies were obtained from the vastus lateralis muscle, under local anesthetic (1% lidocaine), using the percutaneous needle biopsy technique of Bergström, with 5- 6mm needles and manual suction. For RNA extraction, 35 mg of muscle tissue was snap frozen in liquid nitrogen and stored at -80°C. For mononuclear cell isolations, approximately 250 mg of tissue was placed in pre-chilled Ham's F-10 media with 10% horse serum. For immunohistochemical analysis, approximately 100 mg of tissue was embedded in tragacanth gum on cork, frozen in liquid-nitrogen cooled isopentane, and stored at -80°C

### **3.2.3 Animals**

Mice from a Pax7<sup>CreER/+</sup>-tdTomato<sup>fl/+</sup> strain were used in all in vivo studies as part of an ongoing study exploring the role of satellite cell communication during MOV. C57BL/6J mice (obtained from the Jackson Laboratory) were used for macrophage in vitro experiments. Experiments and animal care were performed in accordance with the University of Kentucky Institutional Animal Care and Use Committee. All mice were housed in a temperature- and humidity-controlled room and maintained on a 14:10 light:dark cycle, with standard chow and water ad libitum. All mice were females >4 months old at the time of experimentation.

### **3.2.4 Synergist ablation surgery-induced mechanical overload (MOV) of muscle**

Mice underwent bilateral synergist ablation surgery to induce hypertrophy of the plantaris muscle, as previously described by our laboratory [101]. Briefly, mice were anesthetized using 95% oxygen and 5% isoflurane gas, then approximately 1/3 of the lower

gastrocnemius/soleus complex was removed, careful not to disturb neural or vascular supply. Sham mice were also anesthetized and a similar incision was made followed by immediate suture. Following 4 days of MOV, mice were euthanized via lethal dosage of sodium pentobarbital and cervical dislocation.

### **3.2.5 Mononuclear cell isolation from skeletal muscle**

To isolate mononuclear cells from mouse and human muscle, we used a modified version of the fluorescent activated cell sorting (FACS) protocol from the Rando laboratory [115]. After a single cell suspension was made from fresh muscle using collagenase followed by collagenase and dispase, it was filtered through a 40  $\mu$ m strainer. Propidium iodide (PI) was added to gate out dead cells using an iCyt FACS machine (Sony Biotechnology, Champaign, IL, USA). In mouse, we separated out satellite cells prior to scRNA-seq, which were identified as Vcam<sup>+</sup> (Biolegend, San Diego, CA, USA), and all other PI<sup>-</sup> cells were collected. In human, we used the same digestion protocol to generate a single cell suspension but subsequently used antibodies to identify immune cells, which were labeled and sorted as CD11b<sup>+</sup>/CD45<sup>+</sup>/PI<sup>-</sup> (Biolegend), and used for scRNA-seq.

### **3.2.6 Cell Culture**

Human myogenic progenitor cells (MPCs) were isolated from the gracilis of two patients (1 female and 1 male) undergoing anterior cruciate ligament reconstruction (age 30-34 years) using a CD56 (Biolegend) antibody for FACS. Cells were passaged 2-3 times in growth media consisting of Ham's F-10, 20% fetal bovine serum (FBS, Atlanta Biological, Minneapolis, MN, USA), 1% penicillin/streptomycin and 10ng/ml basic fibroblast growth-factor (bFGF, Peprotech, Rocky Hill, NJ, USA). Cells were

differentiated into myotubes for 5 days using MyoCult differentiation media (DM, Stemcell Technologies, Vancouver, Canada). On the fifth day, fresh media was added just prior to electrical pulse stimulation (EPS). Cells were then either stimulated at 12 V, 1 Hz, 2 ms for 24 hr (IonOptix C-Pace EP, Westwood, MA, USA) or had electrodes placed in wells with no stimulation (E(+) or E(-)), followed by immediate RNA extraction using Qiazol (Qiagen, Hilden, Germany). Conditioned media (CM) was pooled from each 6-well plate and centrifuged at 600xg for 10 min to remove debris and frozen at -80°C.

Bone marrow derived macrophages (BMDM) were obtained from bone marrow (BM) precursor cells as previously described [116]. Briefly, total BM was obtained from mice by flushing femur BM with Dulbecco's modified eagle's media (DMEM). Cells were cultured in DMEM medium with 20% FBS and 10ng/ml colony stimulating factor- 1 (CSF-1, Stemcell Technologies) for 6 days; CSF-1 free media was added on day 7 for 12 hr. CM from myotubes was incubated with goat anti-human LIF neutralizing antibody (0.1 µg/ml, ThermoFisher, Waltham, MA, USA) or control IgG overnight at 4°C with gentle agitation and then diluted 1:1 with Myocult DM. The conditioned media was added on day 7 for 24 hr. Cells were then immediately collected in Qiazol (Qiagen) for RNA extraction.

### **3.2.7 DQ collagen type I assay**

The fluorogenic DQ collagen was used to directly monitor collagenase activity in vitro. Briefly, myotube CM from either E(-) or E(+) was added to BMDM seeded in 12-well plates. 100µg/ml of DQ collagen type I (ThermoFisher) was added to 5 different

conditions; DM only (control), 1:1 CM/DM from E(-) and E(+) myotubes with no BMDM, and 1:1 CM/DM from E(-) and E(+) myotubes with BMDM. Following 120 min, 200  $\mu$ l was removed from each well and added to a 96-well flat bottom plate. To measure the fluorescence intensity, a fluorescence microplate reader equipped with standard fluorescein filters was used. Digestion products from the DQ collagen were measured at an absorption maxima of ~495 nm and fluorescence emission maxima of ~515 nm and corrected for background by subtracting the control from the value derived.

### **3.2.8 Immunohistochemistry**

Human skeletal muscle macrophage identification and quantification were performed according to a detailed and validated method [117]. Briefly, macrophages were identified by stepwise incubation with antibodies against the pan macrophage marker CD11b (Cell Sciences, Newburyport, MA, USA) followed by CD206 (R&D Systems, Minneapolis, MN, USA). Slides were fixed in  $-20^{\circ}\text{C}$  acetone and blocking steps were taken to prevent nonspecific background and cross-reactivity between amplification reagents. Slides were incubated with mouse IgG1 anti-CD11b (1:100, Cell Sciences) in 2.5% normal horse serum (NHS, Vector Laboratories, Burlingame, CA, USA) overnight at  $4^{\circ}\text{C}$ . On the second day, the sections were rinsed in PBS, followed by incubation with goat anti-mouse biotin secondary (1:1,000, Jackson ImmunoResearch, West Grove, PA, USA) for 90 min at room temperature, followed by streptavidin-HRP (ThermoFisher) for 1 hr and then tyramide signal amplification with Alexa Fluor 488 (ThermoFisher) for 15 min. Sections were placed back in streptavidin/biotin blocking kit (Vector Laboratories) and 2.5% NHS for 1 hr and incubated overnight with goat anti-CD206 (1:200, R&D Systems) in 2.5% NHS at  $4^{\circ}\text{C}$ . On the fourth day, sections were incubated in rabbit anti-

goat biotinylated secondary antibody (1:1,000, Jackson ImmunoResearch) for 90 min at room temperature. Streptavidin Alexa Fluor 594 was then added to the section for 1 hr, followed by nuclei visualization with DAPI. 4',6-diamidino-2-phenylindole (DAPI) (ThermoFisher). Slides were coverslipped with Vectashield (Vector Laboratories) and stitched images of whole muscle cross-sections were acquired with a 20× objective on a Zeiss upright microscope (Carl Zeiss, Thornwood, NY, USA). The abundance of all CD11b+CD206+ cells was manually quantified using the event count tool in Zen software (Carl Zeiss) and normalized to number of fibers per cross-section.

To visualize capillaries, frozen muscle sections were dried and rehydrated for 5 min with 1x phosphate buffered saline (PBS), followed by two 5-min washes with PBS. Sections were blocked for 1 hr in 2.5% NHS then incubated for 90 min with a mixture of 2 lectins: biotinylated *Ulex europaeus* (1:200, Vector Laboratories) and biotinylated *Griffonia simplicifolia* (1:200, Vector Laboratories), and anti-laminin (1:200, Millipore Sigma, St. Louis, MO, USA). Sections were then washed and incubated for 1 hr with streptavidin Alexa Fluor 594 (ThermoFisher) to visualize capillaries and anti-rabbit Alexa Fluor 488 (ThermoFisher) to visualize laminin to demarcate fiber borders. After 3 final washes, the slides were coverslipped with Vectashield and imaged. Capillaries were counted manually and expressed per muscle fiber.

Analysis of satellite cell abundance was performed as follows. After drying, sections were fixed in -20°C acetone, washed with PBS, incubated with 3% hydrogen peroxide, and blocked for 1 hr in 2.5% NHS. Satellite cells were labelled by overnight incubation with anti-paired box 7 (Pax7) (Developmental Studies Hybridoma Bank, Iowa City, Iowa, USA). Following PBS washes, sections were incubated with biotinylated anti-



mouse IgG1 (1:1,000 Jackson ImmunoResearch) for 90 min. Washes were repeated followed by a 1 hr incubation with streptavidin-HRP (ThermoFisher). Fluorescent labelling was achieved by incubating with SuperBoost tyramide signal amplification Alexa Fluor 488 (ThermoFisher) in PBS for 20 min. Primary antibody against laminin (Millipore Sigma) was added followed by anti-rabbit Alexa Fluor 594 secondary antibody (ThermoFisher) to visualize and quantify muscle fibers. Sections were washed, incubated for 10 min with DAPI to label nuclei, and coverslipped. Whole cross-section images were acquired with a 20× objective, satellite cells were identified as Pax7+/DAPI+ and expressed per fiber. Laminin immuno-stained images were previously used to determine fiber size [48]. Myonuclear number was determined using rabbit anti-dystrophin (Abcam) followed by anti-rabbit Alexa Fluor 488 secondary antibody (ThermoFisher) and DAPI to visualize and quantify nuclei within the dystrophin border.

### **3.2.9 Gene expression experiments in myotubes and BMDM**

For cellular RNA extraction, cells were lysed in Qiazol reagent (Qiagen), and RNA was extracted using the Zymo MiniPrep kit (Zymo Research, Irvine, CA, USA) with slight modification; the aqueous phase from Qiazol (Qiagen) combined with 3-bromo-chloropropane following phase separation was added directly to the spin column. RNA concentration and quality were assessed via NanoDrop (ThermoFisher) and Bioanalyzer using Nano chips (Agilent, Santa Clara, CA, USA). For real-time PCR of cells, 10 ng of complementary DNA (cDNA) was used per reaction, and reactions were performed using TaqMan chemistry (ThermoFisher) and Taqman probes; *LIF*- Hs01055668\_m1; *Mmp14*-Mm00485054\_m1; *β2-Microglobulin (B2M)*- Hs00187842\_m1; (*B2m*)-

Mm00437762\_m1, on a QuantStudio 3 (ThermoFisher) in duplicate with *B2M* as the housekeeping gene.

For RNA sequencing (RNA-seq), myotube RNA was prepared as a 250–300 bp nonstrand-specific library using the NEBNext Ultra RNA Library Prep Kit (NEB) followed by paired-end sequencing using an Illumina NovaSeq 6000 s4 platform (Novogene, Sacramento, CA). Mapping to the human - hg38 transcriptome (release 100) was performed using STAR, data were normalized to counts per million (CPM) add  $1.0E-4$  per Partek recommendation. Quality was assessed and reads were filtered by removing reads that contained adapters, reads that contained N > 0.1% (N represents base that could not be determined), and low-quality reads (quality value of over 50% of bases of the read  $\leq 20$ ), and differential analysis was performed using Partek Gene set analysis (GSA) tool with default report options.

### **3.2.10 Single cell RNA-sequencing (scRNA-seq)**

The single cell suspension from human and mouse muscles was cleared of debris, dead cells, and doublets via FACS, as described above. The pellet was washed and re-suspended in PBS with 0.04% bovine serum albumin (BSA, Millipore Sigma) to minimize ambient RNA and cellular aggregation, in accordance with 10X Genomics recommendations (10X Genomics, Pleasanton, CA, USA). Cell concentration was determined via hemocytometer prior to being loaded on the 10X Chromium chip. After cells were loaded into the 10X Chromium Controller, the Single Cell 3' reagent kit was applied according to the manufacturer's protocol. Libraries were prepared using version 3.0 chemistry and were sequenced on the Illumina NextSeq 500 platform for mouse and

the Illumina NovaSeq 6000 system for human. The Cell Ranger Single Cell Software Suite was used to perform sample demultiplexing, barcode processing and single cell 3' gene counting (<http://software.10xgenomics.com/single-cell/overview/ddddome>). The cDNA insert was aligned to an appropriate reference genome using STAR. For mouse muscle, mm10 transcriptome (release 93) was used. For human muscle, hg 38 transcriptome (release 100) was used. Partek Flow was used for all downstream analysis from Filtered\_Barcode\_Matrix.h5 files. For the mouse sham sample; 96.89% of reads were within cells, the estimated number of cells was 3,006, with a median gene per cell of 4,007. For the 4-day MOV mouse sample; 99.38% of reads were within cells, the estimated number of cells was 4,494, with a median genes per cell of 5,449. For the post-acute resistance exercise (RE) bout human sample; 81.9% of reads were within cells, the estimated number of cells was 3,919, with a median genes per cell of 2,248. Filter criteria included expressed genes (Min: 400, Max: 6,000) and mitochondrial reads percent (Min: 0%, Max: 15.00%). Additional filtering was performed which excluded features where values were < 1.0 in at least 99.9% of the samples yielding a total of 12,059 genes for downstream analysis. Samples were normalized using counts per million and log transformation. Principal component analysis (PCA) was used prior to Uniform Manifold Approximation and Projection (UMAP) for visual based clustering. All statistical comparisons were conducted in Partek using GSA.

### **3.2.11 Statistical Analyses**

Results are presented as mean  $\pm$  SEM. Data were analyzed with GraphPad Prism software, via a one-way repeated measures ANOVA with Sidak's correction for multiple comparisons or an unpaired two-tailed Student's t-test. Linear regressions employed the

Pearson product-moment correlation coefficient when the two continuous variables were normally distributed (including all figures depicting regressions). Significance was set at a  $P < 0.05$ . False-discovery rates set to  $\text{Adj-}P < 0.05$  were implemented for all scRNA-seq data analyzed.

### **3.3 RESULTS**

#### **3.3.1 The increase in human muscle macrophages following PRT is positively associated with changes in muscle fiber cross-sectional area (CSA), capillary density, myonuclear accretion and satellite cell abundance**

We previously published data from the MASTERS clinical trial demonstrating an increase in macrophages, CSA, and satellite cells comparing baseline and post-14-weeks of PRT biopsies [48]. In the present study, we determined if the change in macrophage abundance was correlated to changes in the other muscle properties. We found a positive association between the percent change in macrophage abundance with CSA ( $r = 0.578$ ,  $P < 0.005$ , Figure 3.1A), myonuclear abundance ( $r = 0.467$ ,  $P < 0.05$ , Figure 3.1B), satellite cells ( $r = 0.421$ ,  $P < 0.05$ , Figure 3.1C), and capillaries ( $r = 0.507$ ,  $P < 0.005$ , Figure 3.1D). Representative immunohistochemistry images used for quantifications of macrophages (CD11b and CD206), satellite cells (Pax7), CSA (Laminin) and myonuclear accretion (Dystrophin/DAPI) and capillaries (Lectin) are shown in Figures 3.2A-D.

Chapter 2 showed that ECM remodeling genes, including *MMP14*, are increased following 14-weeks of PRT [137]. Although the change in macrophage abundance was not correlated to the change in *MMP14* expression with PRT, macrophage and *MMP14*

mRNA abundance were correlated in the post-PRT biopsy (Figure 3.1E,  $r = 0.578$ ,  $P < 0.05$ ).

### **3.3.2 Human skeletal muscle macrophage scRNA-seq transcriptome changes following an acute bout of resistance exercise (RE)**

We sought to verify that muscle macrophages express *MMP14*, as well as other MMP members, and if expression corresponds to any sub-population of macrophages following a single bout of RE. We recruited one participant from the MASTERS Trial to provide a muscle biopsy 24 hr after an acute bout of RE that was processed for scRNA-seq. The muscle biopsy was digested, cells labeled using a combination of CD45, CD11b and PI for FACS, and immediately processed for scRNA-seq. Our sorting strategy captured a variety of different immune cell populations including monocytes, natural killer cells, T-cells, in addition to macrophages (Figure 3.3A). Graph-based clustering identified 10 separate clusters (Fig 3.3B), while the macrophage cloud was divided into 5 separate clusters (Supplementary Table 3.1). In the larger macrophage clusters (1-3), we identified various genes capable of inducing skeletal muscle remodeling, including *MMP14*, *TGF $\beta$ 1*, *VEGFA* and *IGF1* (Figure 3.4A-D). Cluster 1 expressed the highest levels of *IL10*, *MMP14* and *MMP19* (Supplementary Table 3.1). Cluster 2 had the greatest enrichment for *CCL2*, whereas cluster 3 was highest for *CCR2* (marker of infiltrating monocyte/macrophage, Supplementary Table 3.1). In analyzing the data, we found that *MMP14* expression was the most abundant MMP transcript expressed by human muscle macrophages (Supplementary Table 3.1). Based on our published whole muscle RNA-seq

data (see Chapter 2) that identified *MMP14* as significantly elevated following PRT, we attempted to further explore potential mechanisms regulating *Mmp14* expression in mice using synergist ablation, a model of mechanical overload (MOV) in muscle.

### **3.3.3 Mouse MOV induced changes in macrophage sub-populations, activation and *MMP14* expression**

To gain further insight into the changes that occur with MOV in macrophages, as well as other resident mononuclear cells, we performed synergist ablation surgery to induce skeletal muscle hypertrophy of the plantaris. Sham and 4 day MOV mouse plantaris muscle was enzymatically digested and sorted on all live cells excluding satellite cells and processed for scRNA-seq analysis. Using well-known cell type-specific markers, scRNA-seq analysis identified fibrogenic adipogenic progenitor cells (FAPs), endothelial cells, macrophages, T cells, myonuclei and neutrophils for both Sham and MOV samples (Figures 3.5A and B). The cell type distribution changed dramatically with MOV when controlling for total cells analyzed per sample (Sham= 2430 cells and MOV= 4098 cells). The proportion of mononuclear cells per cell type shifted from Sham to MOV as follows; 67.48% → 6.37% FAPs, 19.54% → 4.22% endothelial cells, 10.08% → 54.65% macrophages, 2.32 → 2.29% T cells, and 0.57% → 32.48% neutrophils (Figure 3.5C).

The robust increase in macrophage proportion, as demonstrated by the re-classification of macrophages using UMAP (Figure 3.6A), was subjected to unbiased graph-based clustering (Figure 3.6B). Unbiased cluster analysis of MOV and Sham macrophages identified 7 clusters (Figure 3.6B, Supplementary Table 3.2) with Sham macrophages

clustering separately (cluster 7). The most notable differences observed were the enrichment of resident macrophage markers in cluster 7 and markers of infiltration in cluster 4 (Supplementary Table 3.2). When comparing Sham to MOV macrophages, we observed 2794 differentially expressed genes (DEG) as visualized by volcano plot (Figure 3.6C). Those genes that demonstrated the most profound upregulation with MOV were *Arg1*, *Thbs1*, *Cxcl3*, *Slpi*, *Spp1*, and *Mmp14* (Adj-P <0.05, Supplementary Table 3.2). Genes that were significantly higher in Sham compared to MOV mice were *Retnla*, *Cd209* (*f,d,b and g*), *Lyz1*, *Pla2g2d*, and *Cxcl13* (Adj-P <0.05, Supplementary Table 3.2).

When assessing whether *Mmp14* expression was specific to any graph-based cluster (Figure 3.6D), we observed that cluster 2 and 3 both demonstrated elevated *Mmp14* expression (Supplementary Table 3.2); however, visually, *Mmp14* mRNA was more apparent throughout the entire macrophage cloud (Figure 3.6D) than previously observed with human macrophages 24 hr after the RE bout. Furthermore, tissue inhibitor of metalloproteinases 2 and 3 (*Timp2/3*, inhibitors of *Mmp14*), were significantly decreased in MOV mice compared to Sham (Supplementary Table 3.2). When assessing *Mmp14* expression changes across all cell types, we found that the predominate source of *Mmp14* expression was FAPs (Figure 3.6E). However, following 4 days of MOV, we found that proportionally, macrophages dramatically increased their expression of *Mmp14* (Figure 3.6E). The proportion of mononuclear cells expressing >1 *Mmp14* from Sham to MOV is as follows; 98.2% → 14.35% FAPs, 1.61% → 4.72% Endothelial cells, 0.23% → 79.10% macrophages, 0.00% → 0.07% T cells, and 0.00% → 1.70% neutrophils (Figure 3.6E). If these findings translate to humans, this might explain why we did not observe a

correlation between the change in *MMP14* and macrophages with PRT but were able to identify an association at the end of 14-weeks PRT.

In identifying whether *Mmp14* expression was derived from newly infiltrating cells following MOV, we compared *Mmp14* mRNA positive macrophages (1 >*Mmp14*, *Mmp14*(+)) vs. *Mmp14* mRNA negative macrophages (1 <*Mmp14*, *Mmp14*(-)) in the MOV sample. GSA generated 1517 DEG (Adj-P <0.05, Supplementary Table 3.3) between *Mmp14*(+) and *Mmp14*(-) macrophages. Markers of infiltrating macrophages (*Ccr2* and *Ly6c2*) were significantly higher in the *Mmp14*(-) compared to *Mmp14*(+) macrophages (Adj-P <0.05, Supplementary Table 3.3).

### **3.3.4 LIF mediates increases in *MMP14* expression in bone marrow derived macrophages (BMDM) in response to EPS-stimulated myotube conditioned media (CM)**

To gain further insight into the mechanisms regulating *Mmp14* expression in vivo, we used an in vitro exercise mimetic, electrical pulse stimulation (EPS), to induce chronic myotube contractions for a 24 hr period. Previous research has shown that EPS induces both myotube hypertrophy [118], as well as increases in cytokine levels [119]. In attempting to identify muscle-derived cytokines upregulated by muscle contraction, we performed RNA-seq on two different primary human cell lines comparing EPS stimulated (E(+)) to non-stimulated control (E(-)) myotubes. Due to the low N, we used fold change cut-offs of >1.5 and unadjusted P <0.05 to identify potential cytokines that were upregulated following 24 hr of EPS (Supplemental Table 3.4). We identified LIF as



one potential cytokine upregulated with E(+), previously reported to induce the degradation of p53, a repressor of *MMP14* [113, 114]. We validated our RNA-seq findings with real-time PCR in two human cell lines, performed in triplicate (Figure 3.7A,  $P < 0.05$ ). Next, we sought to determine if LIF influenced *Mmp14* expression. Following 24 hr of E(+) or E(-), we collected myotube CM and treated BMDM for 24 hr using both E(+) and E(-) conditions. In parallel wells, a human anti-LIF neutralizing antibody (LIFAb+/-) was added to CM prior to treating BMDM. Following 24 hr, BMDM RNA was collected immediately and real-time PCR was performed using probes for *Mmp14*. Treatment of BMDM with E(+)LIFAb(-) CM resulted in a significant increase in *Mmp14* expression compared to E(-)LIFAb(-) CM (Figure 3.7B,  $P < 0.05$ ). However, in the presence of the anti-LIF neutralizing antibody, E(+)LIFAb(+) CM failed to induce a significant increase in *Mmp14* expression in BMDM cells (Figure 3.7B).

### **3.3.5 BMDM treated with EPS conditioned media display enhanced type I collagen degradation**

To determine if elevated *Mmp14* expression in BMDM by E(+)LIFAb(-) CM results in collagen degradation, we used an in vitro model to assess type I collagen degradation using the DQ Collagen 1 assay, which emits fluorescein as collagen is degraded. We first assessed if myotube CM following E(+) or E(-) induced any significant changes above control DM. We detected very little fluorescein emission when the collagen was treated with E(+/-) CM alone. BMDMs treated with E(+/-)LIFAb(+/-) showed a significant increase in fluorescein across all groups compared to E(+/-) CM alone (no cells, Figure 3.8,  $P < 0.0001$ ). However, E(+)LIFAb(-) CM treated BMDM showed a significant increase in fluorescein above what was observed from E(-)LIFAb(+/-) CM treated

BMDM, (Figure 3.8,  $P < 0.05$ ). CM treatment with the anti-LIF neutralizing antibody (E(+)/LIFAb(+)), prevented the increased degradation rates observed in E(+)/LIFAb(-) CM treated BMDM (Figure 3.8).

### 3.4 Discussion

The primary findings of this study demonstrate a novel interaction between skeletal muscle fibers and macrophages following mechanical overload that may mediate ECM remodeling, potentially mediated by MMP14. We provide several novel discoveries in both humans and mice using various modalities to demonstrate the cross-species conservation of our findings. These experiments were based on our findings, presented in Chapter 2, that PRT induces substantial transcriptomic changes to ECM remodeling pathways [137], as well as the association between changes in macrophage abundance and changes in ECM remodeling genes in response to exercise we reported previously [44]. At the end of 14-weeks of PRT, we found that macrophage abundance is significantly correlated to MMP14 mRNA levels. The change in muscle macrophages with PRT is also positively associated with changes in muscle fiber CSA, satellite cells, capillaries and myonuclei following 14-weeks of PRT. *MMP14* expression increases 1.6-fold following 14-weeks of PRT in older adults, with a more robust change in *Mmp14* expression observed following 4 days of MOV in mouse macrophages. We also observed a concomitant decrease in *Mmp14* inhibitors (*Timp 2 and 3*), which addresses the potential question of whether known inhibitors of MMP14 mitigate this response [120]. MMP14 has been reported to play an important role in myogenesis, angiogenesis, cell migration and the degradation of collagens [111, 113, 121]. When looking for potential regulators of *Mmp14* expression with MOV, we identified LIF, which has been shown to

increase with MOV in mice [122]. No mononuclear cell population increased *Lif* expression by scRNA-seq, suggesting the higher *Lif* expression observed in response to MOV occurred within the myofibers. Therefore, we utilized an in vitro model of RE (EPS) using human primary myotube cultures to induce *LIF* expression and treated BMDM with E(+/-) CM to determine if myotube-derived LIF is capable of promoting BMDM *Mmp14* expression.

Skeletal muscle research aimed at identifying the importance of macrophage activation/function with exercise has been largely correlative in nature [44, 123, 124]. To date only one study has directly demonstrated that macrophage recruitment is necessary for skeletal muscle hypertrophy in mice following MOV [39]. Although we have begun to understand the mechanisms by which macrophages are recruited from the circulation via muscle contraction [125], we have little empirical data to support a mechanism for how MOV may augment resident macrophage activation and promote muscle growth or remodeling. Our lab has recently demonstrated significant macrophage accretion following PRT in healthy older adults [48]. We provide further evidence that macrophage accretion is positively associated with muscle adaptations following PRT such as muscle hypertrophy, satellite cell proliferation, angiogenesis and myonuclear accretion. Moreover, this positive relationship between changes in macrophage abundance and muscle hypertrophy may play a pivotal role in older adults who are susceptible to certain aspects of anabolic resistance. From our data, it is apparent that not all subjects responded favorably in terms of growth to 14-weeks of PRT, however, those that displayed the greatest improvements in CSA also displayed the greatest increase in macrophage

abundance. The data generated from our scRNA-seq analysis of one healthy older adult following an acute bout of RE suggests that macrophages may supplement crucial growth factors such as VEGFA, which we have previously identified as lower in healthy older adults compared to young [137].

ScRNA-seq is an attractive approach to identify heterogeneity within cell types, especially macrophages, which have classically been defined in terms of inflammatory vs anti-inflammatory phenotypes. We did not observe any overt classical inflammatory macrophage clusters following an acute bout of RE in our one human subject. Interleukin 1b (*IL1b*) was detected in two clusters, however, those clusters were observed to consist of cells relegated to the monocyte cluster. The majority of macrophages expressed resident macrophage markers such as *LYVE1*, *CD206*, and *CD163* [21]. This is consistent with our previous immunohistochemical data demonstrating a high degree of overlap between the pan-markers CD68/CD11b and alternatively activated (M2) markers CD206/CD163 [117]. When attempting to identify macrophage heterogeneity in mice following MOV, the most notable differences were driven by a subset expressing markers of infiltrating macrophages (*Ccr2* and *Ly6c2*), as well as *Il1b*. However, this cluster (cluster 4) also expressed high levels of the alternatively activated macrophage marker chitinase-like 3 (*Chil3* or *Ym1*).

MOV is similar to muscle regeneration in that it is a potent stimulus for macrophage infiltration [126]. MOV differs from muscle injury models by maintaining muscle fiber

integrity and therefore requires a more subtle approach to ECM remodeling, not requiring removal of necrotic fibers and apoptotic cells. The importance of ECM remodeling with MOV-induced skeletal muscle hypertrophy is thought to be necessary for permitting myofiber expansion through the remodeling of the basement membrane [103]. In human studies, a single bout of exercise did not increase skeletal muscle mRNA levels of *MMP14* [127]. However, following 10 days of training, *MMP14* expression was significantly increased, as well as following 14-weeks of PRT [128]. Synergist ablation MOV in mice has also been shown to increase *Mmp14* expression in the whole muscle [12], and we propose that this is largely driven by the specific increase in *Mmp14* expression from macrophages. Another interesting finding is that human monocytes do not appear to express high levels of *MMP14* according to scRNA-seq. In line with this finding, it appears that in mice *Mmp14*(+) macrophages express significantly lower levels of *Ccr2* and *Ly6c2*, markers of infiltrating monocytes, compared to *Mmp14*(-) macrophages. These results suggest that infiltrating monocytes/macrophages do not enter skeletal muscle primed with high levels of *MMP14* and instead require distinct cues from skeletal muscle to upregulate transcription of *MMP14*.

Exercise-induced myokines (muscle secreted cytokines) are attractive therapeutic targets due to their ability to induce beneficial effects in other cells, tissues and organs [129]. LIF has previously been described as resistance exercise-induced myokine [130], and despite being below detection levels in plasma, LIF is believed to exert local effects following MOV. In addition, LIF knockout mice fail to undergo skeletal muscle hypertrophy following 21 days of MOV, and although the authors did not provide a

mechanism by which LIF promotes skeletal muscle hypertrophy [122]. Our results suggest an important function of LIF that may facilitate the remodeling of the ECM through effects on macrophages. LIF increased *Mmp14* in muscle macrophages, which we validated in vitro using an anti-LIF neutralizing antibody. The mechanism by which LIF potentially regulates MMP14 gene expression was first discovered in a HCT116 cell line (human colorectal cancer cell line), where authors reported an increase in p53 degradation with LIF treatment [114]. In a similar study, IL6 treatment, which is very homologous to LIF, was used to further describe the mechanism by which p53 degradation enables Sp1 binding to the MMP14 gene promoter in HCT116 cells [113]. Sp1 has been previously characterized as the primary transcription factor responsible for MMP14 gene expression in humans [131]. This was illustrated using a luciferase reporter gene driven by the MMP14 promoter, that lacked the Sp1 binding site. This deletion reduced luciferase activity by 90%, which indicated an essential role for Sp1 in maintaining MMP14 transcription [131].

Ultimately our focus was to identify how changes in the muscle macrophage transcriptome with RE/MOV influence ECM remodeling. Despite illustrating enhanced type I collagen degradation following E(+) CM treatment of BMDM in vitro, further studies will be needed in vivo using macrophage-specific *Mmp14* knockout mice to assess the physiological impact of macrophage *Mmp14* on ECM remodeling. Similarly, one could also identify the role of *Mmp14* in targeting pro-*Mmp2* with MOV, as *Mmp2* knockout mice fail to grow in response to MOV [103]. This study provides a myriad of data for those interested in the muscle macrophage response to MOV, and although our

focus was on ECM remodeling, other relevant pathways such as metabolism and toll-like receptor signaling were affected by MOV in muscle macrophages. Transgene insertion of *Lif* driven by *Cd11b* promoter has recently been demonstrated to ameliorate Duchene's muscle dystrophy in mice [132]. Taking advantage of how macrophages are recruited to damaged or exercised muscle makes similar approaches highly attractive. Deepening our understanding of macrophage function will enable future research to manipulate and potentially enhance these responses to reduce skeletal muscle fibrosis and anabolic resistance.

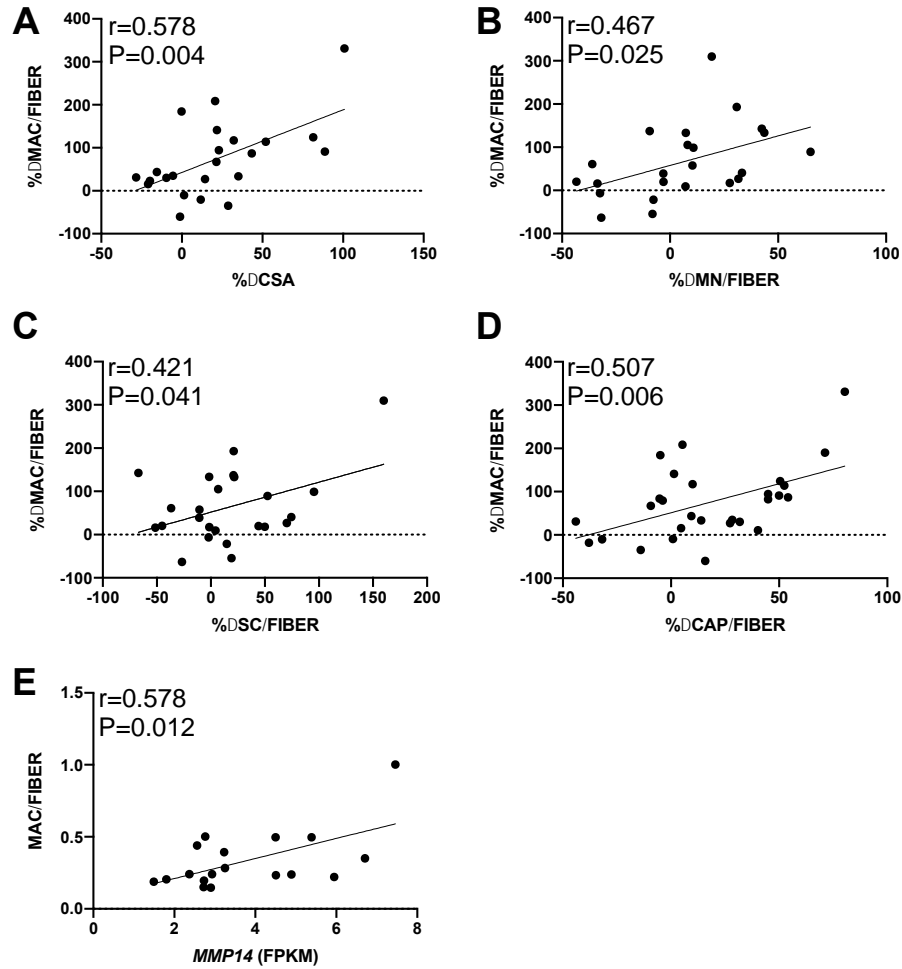


Figure 3.1 In human *vastus lateralis*, Pearson  $r$  correlation analysis demonstrates a significant association between changes in macrophage abundance and changes in (A) muscle fiber CSA ( $r=0.578$ ,  $p=0.004$ ,  $N=23$ ), (B) MN ( $r=0.467$ ,  $P=0.02$ ,  $N=23$ ), (C) SC ( $r=0.421$ ,  $P=0.04$ ,  $N=24$ ), and (D) CAP ( $r=0.507$ ,  $P=0.0059$ ,  $N=24$ ) following 14-weeks of PRT. (E) Absolute number of macrophages correlates to *MMP14* expression at the end of PRT ( $r=0.578$ ,  $P=0.01$ ,  $N=18$ ). CSA, cross-sectional area; MN, myonuclei; SC, satellite cells; CAP, capillaries; *MMP14*, matrix metalloproteinase 14; PRT, progressive resistance exercise training; FPKM, fragments per kilobase of transcript per million mapped reads.



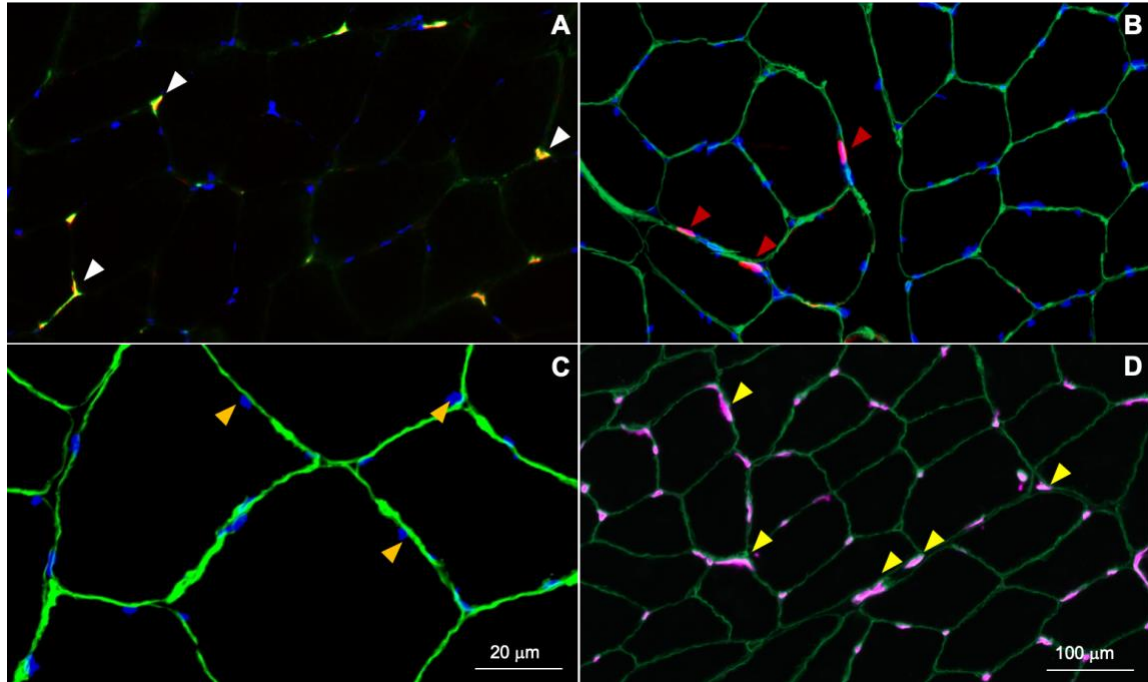


Figure 3.2 Representative images of skeletal muscle immunohistochemistry. (A) Skeletal muscle macrophages were identified using antibodies against CD11b (green) and CD206 (red); CD11b+/CD206+ cells were counted (white arrows). (B) Satellite cells were identified using a Pax7 antibody (red) within the laminin border (green); satellite cells were expressed per fiber. (B) Muscle fiber cross-sectional area was measured using laminin (green) to outline fiber borders. (C) myonuclei were identified as DAPI+ (blue) nuclei within the dystrophin border (gold arrows). (D) Capillaries were identified using antibodies against lectin (pink) with laminin (green) and measured per fiber (yellow arrows). Scale bar=100μm for A, B, and D; scale bar=20μm in C.

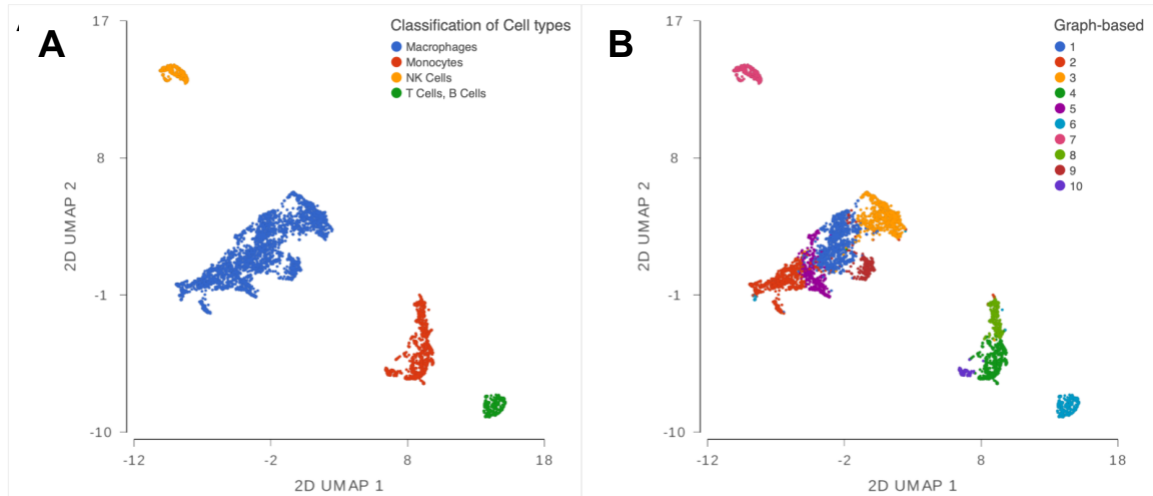


Figure 3.3 scRNA-seq of CD11b+/CD45+ sorted cells derived from human *vastus lateralis* 24 hr after an acute bout of RE. (A) Classification of cell types using gene expression markers identified 5 primary cell types; macrophages (blue), monocytes (red), NK cells (gold) and T cells /B cells (green). (B) Unbiased graph-based clustering identifies 10 clusters in human skeletal muscle immune cell populations with 5 macrophage sub-clusters. Data represented using UMAP. UMAP, Uniform Manifold Approximation and Projection; NK cells, natural killer cells; RE, resistance exercise; scRNA-seq, single cell RNA-sequencing.

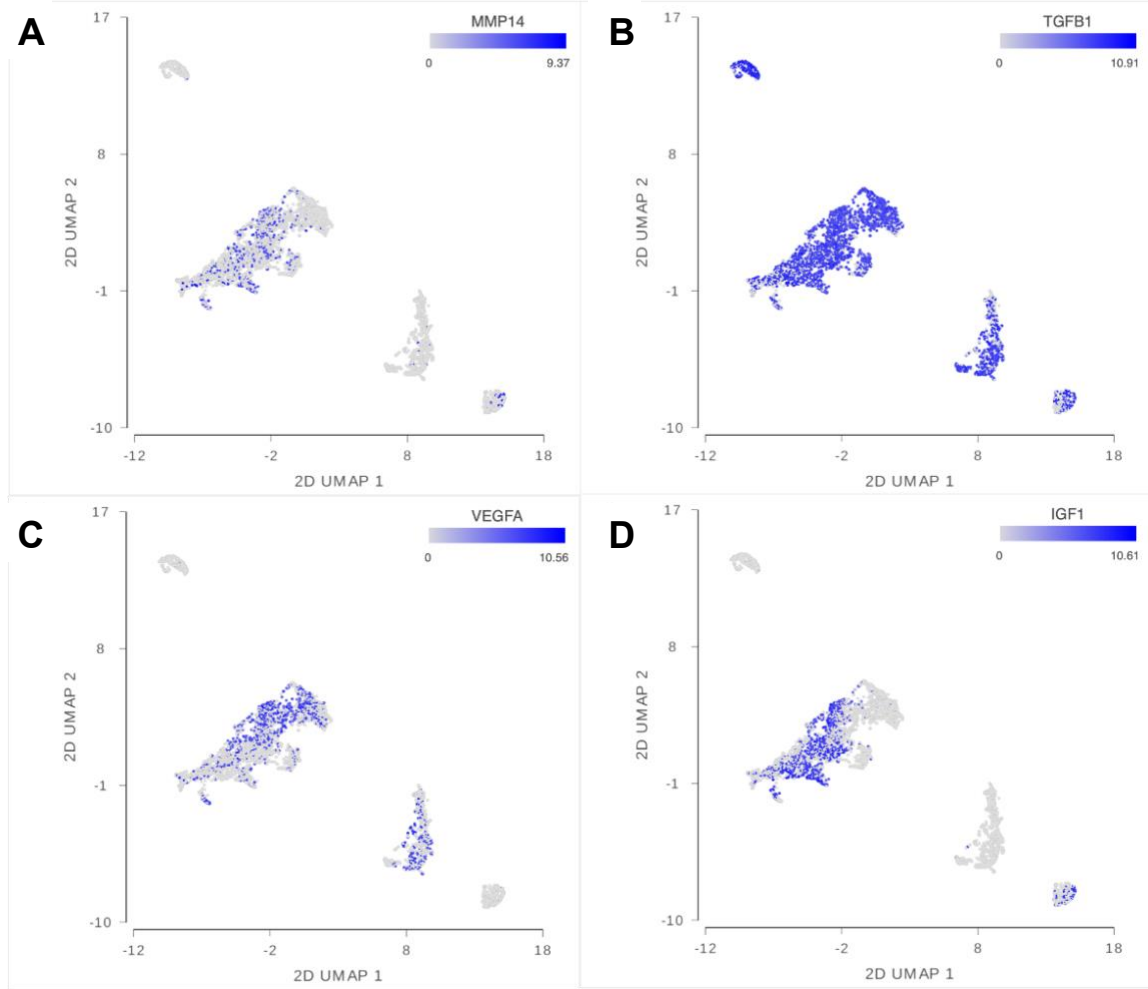


Figure 3.4 scRNA-seq analysis of (A) *MMP14*, (B) *TGFβ1*, (C) *VEGFA*, and (D) *IGF1* as potential macrophage-derived regulators of ECM remodeling, angiogenesis, muscle hypertrophy and satellite cell proliferation/fusion. Data represented using UMAP. Scale bar represents linear expression levels. UMAP, Uniform Manifold Approximation and Projection; MMP14, matrix metalloproteinase 14; TGFβ1; transforming growth factor beta-1; VEGFA, vascular endothelial growth factor A; IGF1, insulin-like growth factor-1; ECM, extracellular matrix; scRNA-seq, single cell RNA-sequencing.

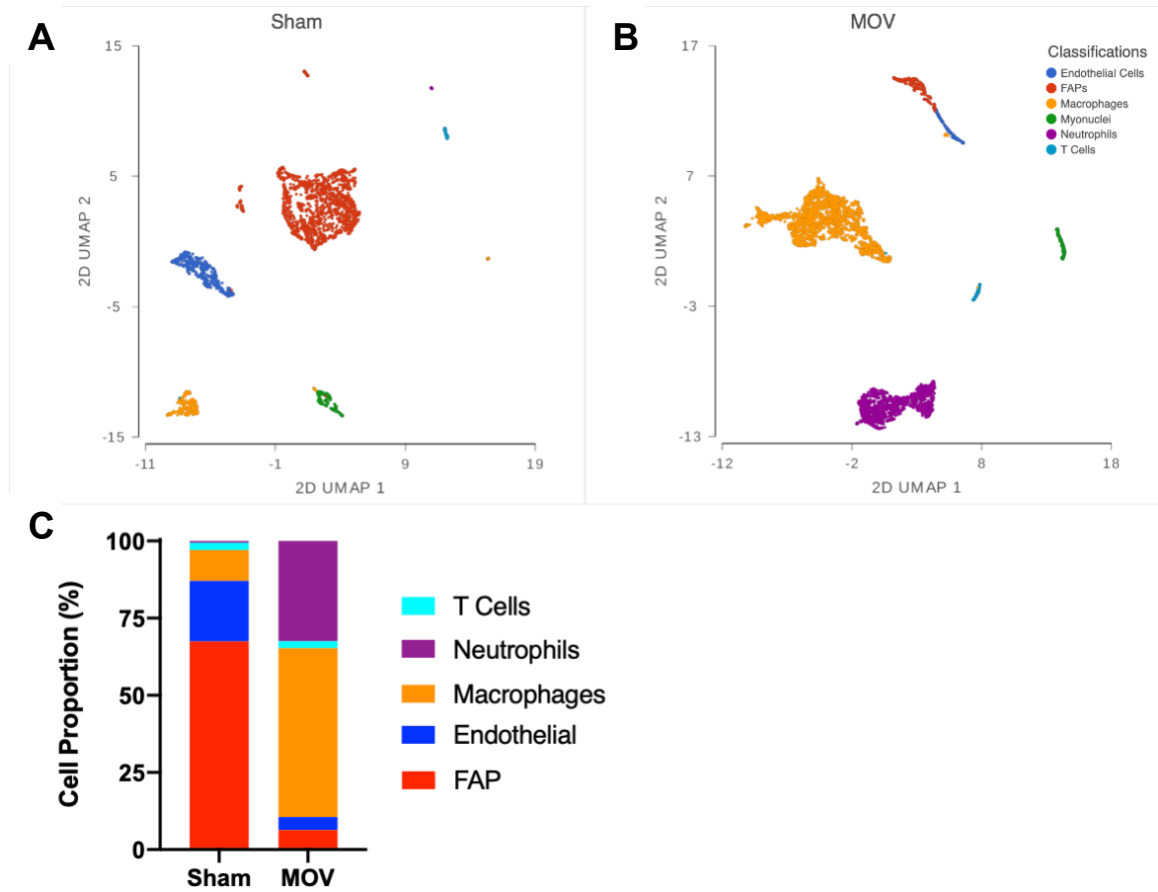
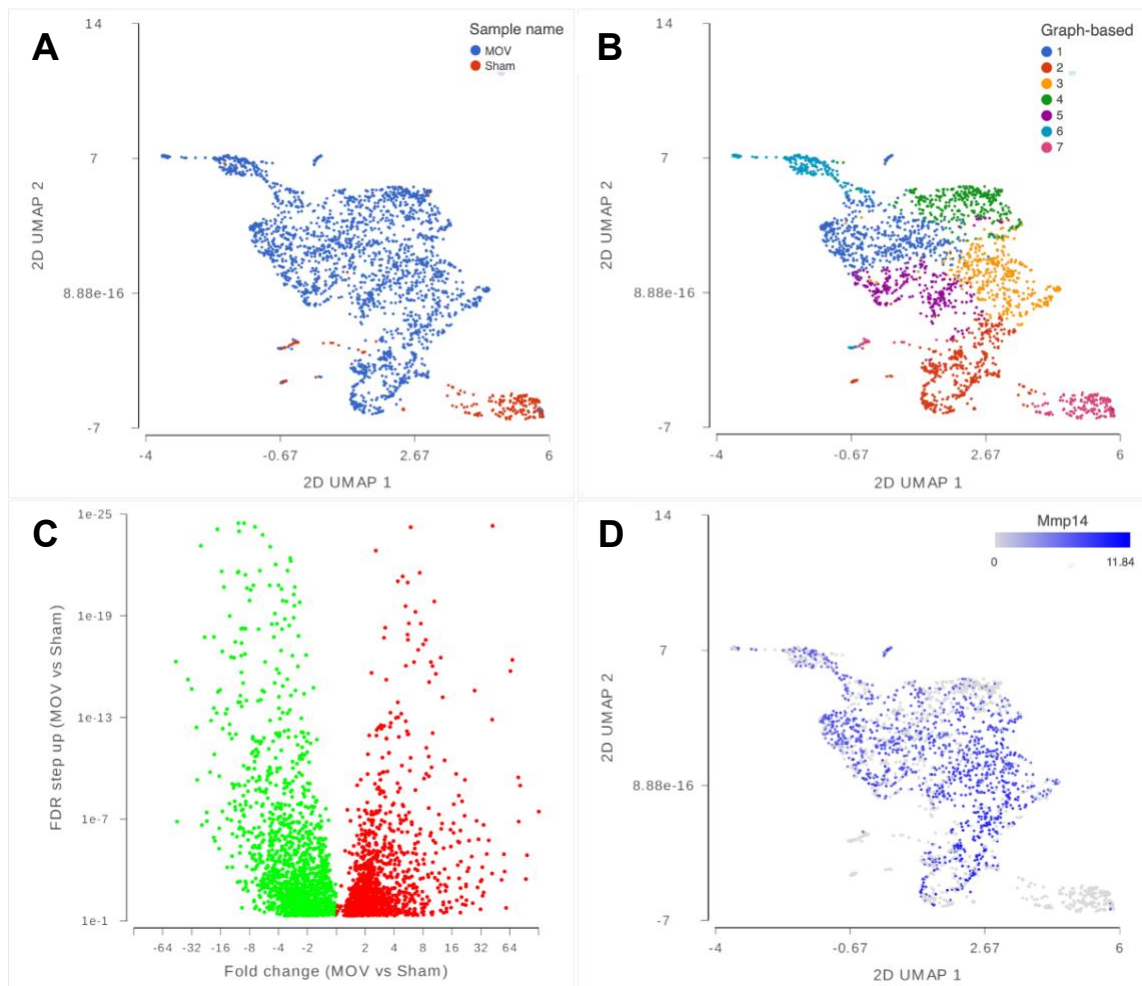


Figure 3.5 scRNA-seq demonstrates dynamic changes in cell populations following 4 days of mechanical overload (MOV) in mouse plantaris using UMAP. Cell types were classified as either endothelial cells, myonuclei, fibrogenic adipogenic progenitors (FAPs), macrophages, neutrophils or T cells under (A) Sham or (B) MOV conditions. (C) Shift in cell type proportions following 4 days of MOV accounting for the total number of cells sorted per sample. N=6,528 total cells (Sham= 2,430 cells and MOV=4,098 cells). scRNA-seq, single cell RNA-sequencing; UMAP, Uniform Manifold Approximation and Projection.



## E **MMP14 Positive Cells**

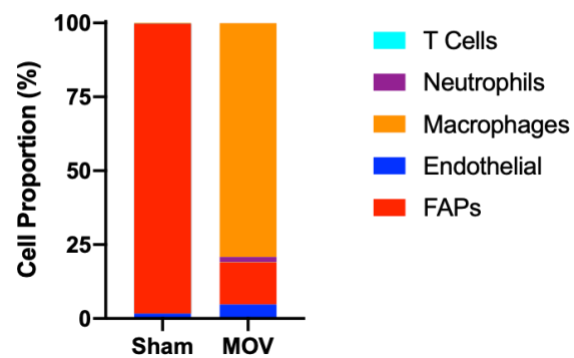


Figure 3.6 scRNA-seq of mouse macrophage populations under Sham and mechanical overload (MOV) conditions. (A) UMAP plot of macrophages under Sham conditions (red) compared to after 4 days of MOV (blue) in mouse plantaris muscle. (B) Unbiased graph-based clustering of macrophages from both sham and MOV muscles reveals 7 sub-clusters with Sham clustering separately (pink). (C) Volcano plot demonstrating the number of differentially expressed genes (DEG) significantly increased (red) or decreased (green) when comparing MOV vs Sham (Adj-P <0.05). (D) *Mmp14* expression (blue) in macrophages across MOV and Sham samples. N=2,382 (sham=230 and MOV=2,152). Assessing *Mmp14* expression across cell types in Sham and 4 day-overloaded muscles. (E) Under Sham conditions, FAPs are the predominate source of *Mmp14* expressing cells, however, following MOV macrophages present as the majority *Mmp14* expressing cells. N=2,396 total cells (sham= 870 cells and MOV=1,526 cells). scRNA-seq, single cell RNA-sequencing; UMAP, Uniform Manifold Approximation and Projection; Mmp14, matrix metalloproteinase 14; FAPs, fibrogenic adipogenic progenitors.

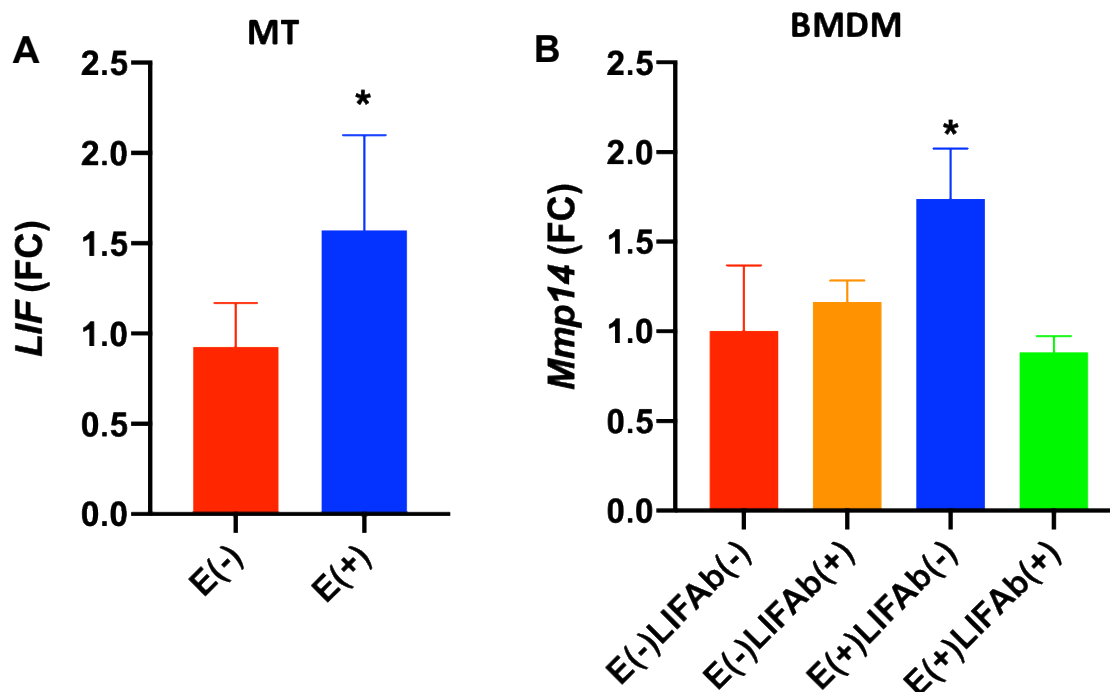


Figure 3.7 BMDM require LIF upregulation in CM from EPS treated myotubes to induce *Mmp14* expression. (A) RNA was isolated from human primary myotubes (MT) subjected to EPS for 24 hr (E(+)) and from unstimulated MTs (E(-)). LIF mRNA was quantified by real-time PCR (\*P < 0.05), using an un-paired students t-test. N=6. (B) CM from E(+) and E(-) MTs was pre-treated with 0.1  $\mu$ g/ml of human anti-LIF neutralizing antibody or IgG control antibody (LIFAb(+/-)) followed by incubation with BMDMs for 24 hr. Cells were collected, RNA isolated and *Mmp14* expression quantified by real-time PCR. Data are expressed as mean  $\pm$  standard deviation. (\*P < 0.05). N=6. Results are expressed as fold change from control group; E(-)LIFAb(-), using one-way repeated measures ANOVA with Sidak's correction for multiple comparisons. MT, myotubes; EPS, electrical pulse stimulation; E(+/-), +/- EPS; BMDM, bone marrow derived macrophages; CM, conditioned media; Mmp14, matrix metalloproteinase 14; LIF, leukemia inhibitory factor.

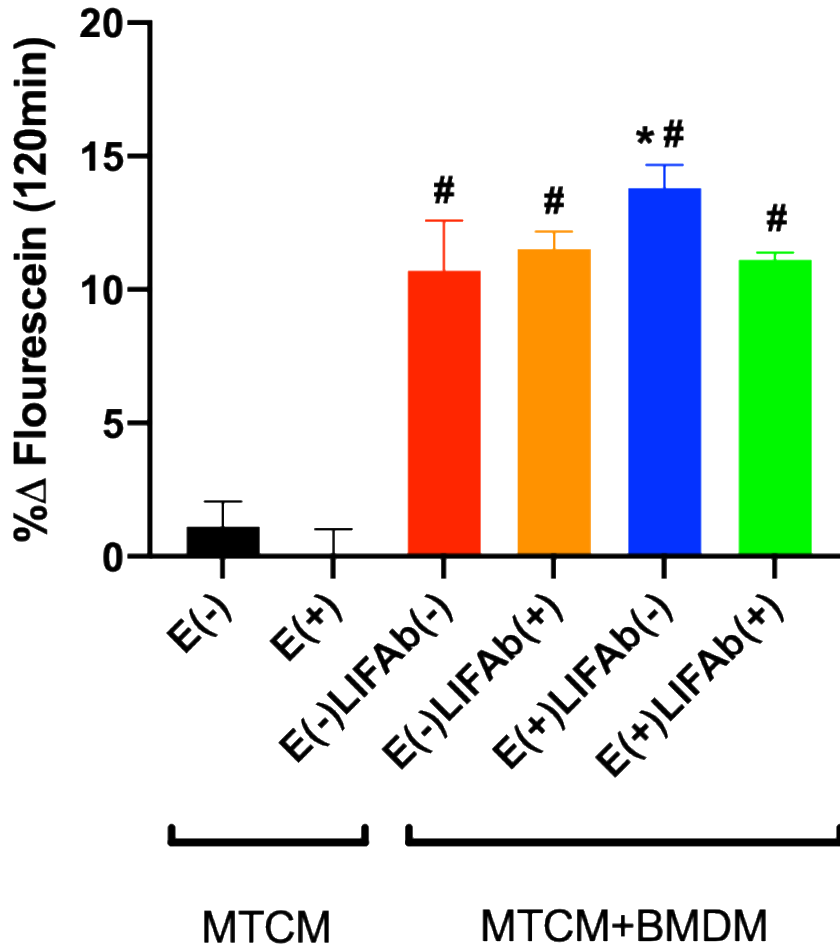


Figure 3.8 Elevated rates of type I collagen degradation in BMDM is influenced by LIF from E(+) CM. DQ Type I Collagen substrate was used to measure the degradation rates of BMDM in the presence of myotube conditioned media (MTCM). BMDM had a significant effect on type I collagen degradation compared to MTCM alone ( $^{\#}P < 0.05$ ). E(+) CM treatment of BMDM (E(+)-LIFAb(-)) had a significant effect above that observed in control group (E(-)-LIFAb(-),  $^{*}P < 0.05$ ). All analysis was performed using one-way repeated measures ANOVA with Sidak's correction for multiple comparisons. N=6 per group. ( $^{\#}P < 0.05$ ) compared to MTCM.  $^{*}P < 0.05$  compared to control BMDM group. BMDM, bone marrow derived macrophages; LIFAb, LIF neutralizing antibody; E(+/-), +/- EPS; EPS, electrical pulse stimulation; LIF, leukemia inhibitory factor.



## CHAPTER 4. CONCLUDING REMARKS AND FUTURE DIRECTIONS

### 4.1 Summary of findings regarding the regulation of ECM with MOV

Progressive resistance exercise training (PRT) is a potent stimulus for a variety of skeletal muscle adaptations that produce beneficial functional outcomes. To adapt to mechanical loading, skeletal muscle must undergo changes both within the muscle fiber, as well as the surrounding extracellular matrix (ECM). While neuronal input drives muscle activation, the response that ensues is dependent upon a variety of cell types in addition to myogenic cells. Using a mouse model of resistance exercise, synergist ablation-induced mechanical overload (MOV), our lab recently published several findings that suggest potential crosstalk between satellite cells (muscle stem cells) and fibroblasts that mediate collagen expression, a major component of the ECM, during MOV [101]. In addition to this, we have also begun to understand how satellite cells modify the muscle ECM degradation rates through matrix metalloproteinase (MMP) regulation [133]. From an “Omics” perspective, as highlighted in Chapter 2, it is apparent that both ECM synthesis and degradation occur during reorganization in order to promote physiological adaptations to PRT [137]. Our lab has sought to expand our understanding of other potential relevant mononuclear cells and how they contribute to ECM regulation. In Chapter 3, we focused on macrophages, due to their increased abundance following 14-weeks of PRT and positive associations with muscle size, capillary density, and satellite cell activity.

## **4.2 Is ECM turnover necessary for skeletal muscle adaptations to MOV?**

The fundamental question regarding whether ECM remodeling is necessary for proper adaptations to PRT/MOV remains unanswered. Despite the considerable research that has gone into understanding the composition, as well as the regulators of production and degradation, little is known about how ECM deposition and degradation ultimately contribute to muscle adaptations with MOV. Skeletal muscle from aged rats has been shown to produce less contractile force than muscle from young rats, which may contribute to what many have termed “anabolic resistance” in older adults [134]. However, to directly assess the role of ECM turnover, the utilization of a mouse strain that synthesizes type I collagen resistant to collagenase cleavage (point mutations in regions targeted by MMPs that inhibit degradation) would be required [135]. The use of this mouse model with MOV may inform our understanding of how necessary ECM turnover is with the remodeling process and how that ultimately affects changes in force generation, cross-sectional area, capillary number, and satellite cell function in overloaded/exercised muscle.

## **4.3 Skeletal muscle and muscle macrophage crosstalk validation in vivo**

The data presented in Chapter 3 makes a compelling point that MOV influences macrophage activation by driving *Mmp14* expression through LIF secretion. While we attempted to demonstrate that this can have a physiological effect on collagen degradation in vitro, ultimately, the use of an *Mmp14* genetic knockout mouse that is specific to macrophages would still be necessary. The data would provide further evidence that macrophages do play a major role in ECM remodeling with MOV. If

defects to the ECM were observed, one would hypothesize that similar to our satellite cell ablated mice, deficits in muscle hypertrophy would follow.

#### **4.4 Macrophage ablation models to demonstrate global impact with MOV**

Ideally, we would have begun our initial endeavors using a macrophage ablation model similar in approach to our well-published satellite cell ablation model [136, 137]. Skeletal muscle macrophages are said to be both derived from yolk-sac origin, as well as throughout the lifespan, via circulating monocytes [124]. In attempting to employ a diphtheria toxin A mouse crossed to a pan macrophage/monocyte Cre-recombinase specific driver mouse, many researchers, including ourselves, have been unable to ablate macrophages in muscle for extended periods (>3 days) or at very minimal effectiveness [22]. To successfully ablate resident macrophages and inhibit macrophage recruitment, one would need a proven and effective macrophage depletion strain such as the Cd11b-DTR mouse line, which successfully ablates macrophages for up to 3 days before giving rise to a surge in infiltrating monocytes. This mouse strain would then be crossed to a *Ccr2* knockout mouse that inhibits infiltrating monocytes. Then one would be able to delete resident macrophages and prohibit reoccupation by infiltrating monocytes for an extended time. This is necessary for assessing changes in ECM remodeling as excess ECM accumulation does not present itself acutely with injury or MOV.

#### **4.5 Final Remarks**

This work extends the role of macrophages in muscle beyond that of injury and their canonical roles in inflammatory and anti-inflammatory muscle repair. Whereas in response to MOV, heterogeneity exists as resident versus newly infiltrated. The muscle

environment clearly alters macrophage phenotype and may result in a unique macrophage population that promotes ECM remodeling.

## REFERENCES

1. Thorsteinsdottir, S., et al., *The extracellular matrix dimension of skeletal muscle development*. Dev Biol, 2011. **354**(2): p. 191-207.
2. Calve, S., S.J. Odelberg, and H.G. Simon, *A transitional extracellular matrix instructs cell behavior during muscle regeneration*. Dev Biol, 2010. **344**(1): p. 259-71.
3. McKee, T.J., et al., *Extracellular matrix composition of connective tissues: a systematic review and meta-analysis*. Sci Rep, 2019. **9**(1): p. 10542.
4. Kjaer, M., *Role of extracellular matrix in adaptation of tendon and skeletal muscle to mechanical loading*. Physiol Rev, 2004. **84**(2): p. 649-98.
5. Ervasti, J.M. and K.P. Campbell, *A role for the dystrophin-glycoprotein complex as a transmembrane linker between laminin and actin*. J Cell Biol, 1993. **122**(4): p. 809-23.
6. MacDonald, E.M. and R.D. Cohn, *TGFbeta signaling: its role in fibrosis formation and myopathies*. Curr Opin Rheumatol, 2012. **24**(6): p. 628-34.
7. Adhyatmika, A., et al., *The Elusive Antifibrotic Macrophage*. Front Med (Lausanne), 2015. **2**: p. 81.
8. Costa, A.G., et al., *Cathepsin K: its skeletal actions and role as a therapeutic target in osteoporosis*. Nat Rev Rheumatol, 2011. **7**(8): p. 447-56.
9. Jablonska-Trypuc, A., M. Matejczyk, and S. Rosochacki, *Matrix metalloproteinases (MMPs), the main extracellular matrix (ECM) enzymes in collagen degradation, as a target for anticancer drugs*. J Enzyme Inhib Med Chem, 2016. **31**(sup1): p. 177-183.
10. McKleroy, W., T.H. Lee, and K. Atabai, *Always cleave up your mess: targeting collagen degradation to treat tissue fibrosis*. Am J Physiol Lung Cell Mol Physiol, 2013. **304**(11): p. L709-21.
11. Lukjanenko, L., et al., *Genomic profiling reveals that transient adipogenic activation is a hallmark of mouse models of skeletal muscle regeneration*. PLoS One, 2013. **8**(8): p. e71084.
12. Chaillou, T., et al., *Time course of gene expression during mouse skeletal muscle hypertrophy*. J Appl Physiol (1985), 2013. **115**(7): p. 1065-74.
13. Chaillou, T., et al., *Identification of a conserved set of upregulated genes in mouse skeletal muscle hypertrophy and regrowth*. J Appl Physiol (1985), 2015. **118**(1): p. 86-97.
14. Rubenstein, A.B., et al., *Single-cell transcriptional profiles in human skeletal muscle*. Sci Rep, 2020. **10**(1): p. 229.
15. Murray, P.J., et al., *Macrophage activation and polarization: nomenclature and experimental guidelines*. Immunity, 2014. **41**(1): p. 14-20.
16. Stein, M., et al., *Interleukin 4 potently enhances murine macrophage mannose receptor activity: a marker of alternative immunologic macrophage activation*. J Exp Med, 1992. **176**(1): p. 287-92.
17. Braga, T.T., J.S. Agudelo, and N.O. Camara, *Macrophages During the Fibrotic Process: M2 as Friend and Foe*. Front Immunol, 2015. **6**: p. 602.

18. Martinez, C.O., et al., *Regulation of skeletal muscle regeneration by CCR2-activating chemokines is directly related to macrophage recruitment*. Am J Physiol Regul Integr Comp Physiol, 2010. **299**(3): p. R832-42.
19. Shireman, P.K., et al., *MCP-1 deficiency causes altered inflammation with impaired skeletal muscle regeneration*. J Leukoc Biol, 2007. **81**(3): p. 775-85.
20. Davies, L.C., et al., *Tissue-resident macrophages*. Nat Immunol, 2013. **14**(10): p. 986-95.
21. Brezovakova, V. and S. Jadhav, *Identification of Lyve-1 positive macrophages as resident cells in meninges of rats*. J Comp Neurol, 2020. **528**(12): p. 2021-2032.
22. Arnold, L., et al., *Inflammatory monocytes recruited after skeletal muscle injury switch into antiinflammatory macrophages to support myogenesis*. J Exp Med, 2007. **204**(5): p. 1057-69.
23. Liu, X., et al., *Macrophage depletion impairs skeletal muscle regeneration: The roles of regulatory factors for muscle regeneration*. Cell Biol Int, 2017. **41**(3): p. 228-238.
24. Melton, D.W., et al., *Absence of CCR2 results in an inflammaging environment in young mice with age-independent impairments in muscle regeneration*. J Leukoc Biol, 2016. **100**(5): p. 1011-1025.
25. Hunt, T.K., et al., *Studies on inflammation and wound healing: angiogenesis and collagen synthesis stimulated in vivo by resident and activated wound macrophages*. Surgery, 1984. **96**(1): p. 48-54.
26. Rappolee, D.A., et al., *Wound macrophages express TGF-alpha and other growth factors in vivo: analysis by mRNA phenotyping*. Science, 1988. **241**(4866): p. 708-12.
27. Simoes, F.C., et al., *Macrophages directly contribute collagen to scar formation during zebrafish heart regeneration and mouse heart repair*. Nat Commun, 2020. **11**(1): p. 600.
28. Vidal, B., et al., *Fibrinogen drives dystrophic muscle fibrosis via a TGFbeta/alternative macrophage activation pathway*. Genes Dev, 2008. **22**(13): p. 1747-52.
29. Juban, G., et al., *AMPK Activation Regulates LTBP4-Dependent TGF-beta1 Secretion by Pro-inflammatory Macrophages and Controls Fibrosis in Duchenne Muscular Dystrophy*. Cell Rep, 2018. **25**(8): p. 2163-2176 e6.
30. Lluís, F., et al., *Urokinase-dependent plasminogen activation is required for efficient skeletal muscle regeneration in vivo*. Blood, 2001. **97**(6): p. 1703-11.
31. Stepanova, V.V. and V.A. Tkachuk, *Urokinase as a multidomain protein and polyfunctional cell regulator*. Biochemistry (Mosc), 2002. **67**(1): p. 109-18.
32. Chapman, H.A., Jr., J.J. Reilly, Jr., and L. Kobzik, *Role of plasminogen activator in degradation of extracellular matrix protein by live human alveolar macrophages*. Am Rev Respir Dis, 1988. **137**(2): p. 412-9.
33. Rahman, F.A., et al., *Impaired ECM Remodeling and Macrophage Activity Define Necrosis and Regeneration Following Damage in Aged Skeletal Muscle*. Int J Mol Sci, 2020. **21**(13).
34. Varga, T., et al., *Highly Dynamic Transcriptional Signature of Distinct Macrophage Subsets during Sterile Inflammation, Resolution, and Tissue Repair*. J Immunol, 2016. **196**(11): p. 4771-82.

35. Mounier, R., et al., *AMPK $\alpha$ 1 regulates macrophage skewing at the time of resolution of inflammation during skeletal muscle regeneration*. *Cell Metab*, 2013. **18**(2): p. 251-64.
36. Summan, M., et al., *Macrophages and skeletal muscle regeneration: a clodronate-containing liposome depletion study*. *Am J Physiol Regul Integr Comp Physiol*, 2006. **290**(6): p. R1488-95.
37. Zhang, C., et al., *Age-related decline of interferon-gamma responses in macrophage impairs satellite cell proliferation and regeneration*. *J Cachexia Sarcopenia Muscle*, 2020.
38. Du, H., et al., *Macrophage-released ADAMTS1 promotes muscle stem cell activation*. *Nat Commun*, 2017. **8**(1): p. 669.
39. DiPasquale, D.M., et al., *Urokinase-type plasminogen activator and macrophages are required for skeletal muscle hypertrophy in mice*. *Am J Physiol Cell Physiol*, 2007. **293**(4): p. C1278-85.
40. Tonkin, J., et al., *Monocyte/Macrophage-derived IGF-1 Orchestrates Murine Skeletal Muscle Regeneration and Modulates Autocrine Polarization*. *Mol Ther*, 2015. **23**(7): p. 1189-1200.
41. Morey-Holton, E.R. and R.K. Globus, *Hindlimb unloading rodent model: technical aspects*. *J Appl Physiol* (1985), 2002. **92**(4): p. 1367-77.
42. Tidball, J.G. and M. Wehling-Henricks, *Macrophages promote muscle membrane repair and muscle fibre growth and regeneration during modified muscle loading in mice in vivo*. *J Physiol*, 2007. **578**(Pt 1): p. 327-36.
43. Uderhardt, S., et al., *Resident Macrophages Cloak Tissue Microlesions to Prevent Neutrophil-Driven Inflammatory Damage*. *Cell*, 2019. **177**(3): p. 541-555 e17.
44. Walton, R.G., et al., *Human skeletal muscle macrophages increase following cycle training and are associated with adaptations that may facilitate growth*. *Sci Rep*, 2019. **9**(1): p. 969.
45. Yang, C., et al., *Aged cells in human skeletal muscle after resistance exercise*. *Aging* (Albany NY), 2018. **10**(6): p. 1356-1365.
46. Mackey, A.L. and M. Kjaer, *The breaking and making of healthy adult human skeletal muscle in vivo*. *Skelet Muscle*, 2017. **7**(1): p. 24.
47. Jensen, S.M., et al., *Macrophage Subpopulations and the Acute Inflammatory Response of Elderly Human Skeletal Muscle to Physiological Resistance Exercise*. *Frontiers in Physiology*, 2020. **11**(811).
48. Walton, R.G., et al., *Metformin blunts muscle hypertrophy in response to progressive resistance exercise training in older adults: A randomized, double-blind, placebo-controlled, multicenter trial: The MASTERS trial*. *Aging Cell*, 2019: p. e13039.
49. McArthur, S., et al., *Annexin A1 drives macrophage skewing to accelerate muscle regeneration through AMPK activation*. *J Clin Invest*, 2020. **130**(3): p. 1156-1167.
50. Lawrence, T. and G. Natoli, *Transcriptional regulation of macrophage polarization: enabling diversity with identity*. *Nat Rev Immunol*, 2011. **11**(11): p. 750-61.

51. Rowe, G.C., et al., *PGC-1alpha induces SPP1 to activate macrophages and orchestrate functional angiogenesis in skeletal muscle*. Circ Res, 2014. **115**(5): p. 504-17.
52. Larsson, L., et al., *Sarcopenia: Aging-Related Loss of Muscle Mass and Function*. Physiol Rev, 2019. **99**(1): p. 427-511.
53. Han, A., et al., *Diagnostic Criteria and Clinical Outcomes in Sarcopenia Research: A Literature Review*. Journal of clinical medicine, 2018. **7**(4): p. 70.
54. Rosenberg, I.H., *Sarcopenia: origins and clinical relevance*. Clin Geriatr Med, 2011. **27**(3): p. 337-9.
55. Cruz-Jentoft, A.J. and A.A. Sayer, *Sarcopenia*. Lancet, 2019. **393**(10191): p. 2636-2646.
56. Tieland, M., I. Trouwborst, and B.C. Clark, *Skeletal muscle performance and ageing*. J Cachexia Sarcopenia Muscle, 2018. **9**(1): p. 3-19.
57. Hughes, V.A., et al., *Longitudinal changes in body composition in older men and women: role of body weight change and physical activity*. The American Journal of Clinical Nutrition, 2002. **76**(2): p. 473-481.
58. Kim, T.N. and K.M. Choi, *Sarcopenia: definition, epidemiology, and pathophysiology*. Journal of bone metabolism, 2013. **20**(1): p. 1-10.
59. Distefano, G. and B.H. Goodpaster, *Effects of Exercise and Aging on Skeletal Muscle*. Cold Spring Harb Perspect Med, 2018. **8**(3).
60. Gheller, B.J.F., et al., *Understanding Age-Related Changes in Skeletal Muscle Metabolism: Differences Between Females and Males*. Annual Review of Nutrition, 2016. **36**(1): p. 129-156.
61. Petrella, J.K., et al., *Efficacy of myonuclear addition may explain differential myofiber growth among resistance-trained young and older men and women*. Am J Physiol Endocrinol Metab, 2006. **291**(5): p. E937-46.
62. Lavin, K.M., et al., *The Importance of Resistance Exercise Training to Combat Neuromuscular Aging*. Physiology (Bethesda), 2019. **34**(2): p. 112-122.
63. Gharahdaghi, N., et al., *Testosterone therapy induces molecular programming augmenting physiological adaptations to resistance exercise in older men*. J Cachexia Sarcopenia Muscle, 2019.
64. Jakubowski, J.S., et al., *Equivalent Hypertrophy and Strength Gains in beta-Hydroxy-beta-Methylbutyrate- or Leucine-supplemented Men*. Med Sci Sports Exerc, 2019. **51**(1): p. 65-74.
65. Sakashita, M., et al., *Oral Supplementation Using Gamma-Aminobutyric Acid and Whey Protein Improves Whole Body Fat-Free Mass in Men After Resistance Training*. J Clin Med Res, 2019. **11**(6): p. 428-434.
66. McKee, A., et al., *Sarcopenia: An Endocrine Disorder?* Endocr Pract, 2017. **23**(9): p. 1140-1149.
67. Boule, N.G., et al., *Metformin and exercise in type 2 diabetes: examining treatment modality interactions*. Diabetes Care, 2011. **34**(7): p. 1469-74.
68. Malin, S.K. and B. Braun, *Impact of Metformin on Exercise-Induced Metabolic Adaptations to Lower Type 2 Diabetes Risk*. Exerc Sport Sci Rev, 2016. **44**(1): p. 4-11.



69. Baptista, L.C., A.M. Machado-Rodrigues, and R.A. Martins, *Exercise but not metformin improves health-related quality of life and mood states in older adults with type 2 diabetes*. Eur J Sport Sci, 2017. **17**(6): p. 794-804.
70. Flory, J. and K. Lipska, *Metformin in 2019*. JAMA, 2019. **321**(19): p. 1926-1927.
71. Fontaine, E., *Metformin-Induced Mitochondrial Complex I Inhibition: Facts, Uncertainties, and Consequences*. Front Endocrinol (Lausanne), 2018. **9**: p. 753.
72. Hawley, S.A., et al., *The antidiabetic drug metformin activates the AMP-activated protein kinase cascade via an adenine nucleotide-independent mechanism*. Diabetes, 2002. **51**(8): p. 2420-5.
73. Cameron, A.R., et al., *Anti-Inflammatory Effects of Metformin Irrespective of Diabetes Status*. Circ Res, 2016. **119**(5): p. 652-65.
74. Rena, G., D.G. Hardie, and E.R. Pearson, *The mechanisms of action of metformin*. Diabetologia, 2017. **60**(9): p. 1577-1585.
75. Valencia, W.M., et al., *Metformin and ageing: improving ageing outcomes beyond glycaemic control*. Diabetologia, 2017. **60**(9): p. 1630-1638.
76. Rena, G. and C.C. Lang, *Repurposing Metformin for Cardiovascular Disease*. Circulation, 2018. **137**(5): p. 422-424.
77. Heckman-Stoddard, B.M., et al., *Repurposing metformin for the prevention of cancer and cancer recurrence*. Diabetologia, 2017. **60**(9): p. 1639-1647.
78. Rotermund, C., G. Machetanz, and J.C. Fitzgerald, *The Therapeutic Potential of Metformin in Neurodegenerative Diseases*. Frontiers in endocrinology, 2018. **9**: p. 400-400.
79. Barzilai, N., et al., *Metformin as a Tool to Target Aging*. Cell Metab, 2016. **23**(6): p. 1060-5.
80. Farr, S.A., et al., *Metformin Improves Learning and Memory in the SAMP8 Mouse Model of Alzheimer's Disease*. J Alzheimers Dis, 2019. **68**(4): p. 1699-1710.
81. Malin, S.K., et al., *Independent and combined effects of exercise training and metformin on insulin sensitivity in individuals with prediabetes*. Diabetes care, 2012. **35**(1): p. 131-136.
82. Sharoff, C.G., et al., *Combining short-term metformin treatment and one bout of exercise does not increase insulin action in insulin-resistant individuals*. Am J Physiol Endocrinol Metab, 2010. **298**(4): p. E815-23.
83. Braun, B., et al., *Impact of metformin on peak aerobic capacity*. Appl Physiol Nutr Metab, 2008. **33**(1): p. 61-7.
84. Viskochil, R., et al., *Exercise training and metformin, but not exercise training alone, decreases insulin production and increases insulin clearance in adults with prediabetes*. J Appl Physiol (1985), 2017. **123**(1): p. 243-248.
85. Konopka, A.R., et al., *Metformin inhibits mitochondrial adaptations to aerobic exercise training in older adults*. Aging Cell, 2019. **18**(1): p. e12880.
86. Zahn, J.M., et al., *Transcriptional profiling of aging in human muscle reveals a common aging signature*. PLoS Genet, 2006. **2**(7): p. e115.
87. Su, J., et al., *A novel atlas of gene expression in human skeletal muscle reveals molecular changes associated with aging*. Skeletal muscle, 2015. **5**: p. 35-35.

88. Long, D.E., et al., *Metformin to Augment Strength Training Effective Response in Seniors (MASTERS): study protocol for a randomized controlled trial*. *Trials*, 2017. **18**(1): p. 192.
89. Stec, M.J., et al., *Randomized, four-arm, dose-response clinical trial to optimize resistance exercise training for older adults with age-related muscle atrophy*. *Exp Gerontol*, 2017. **99**: p. 98-109.
90. Andrews, S., *FastQC: a quality control tool for high throughput sequence data*. 2010.
91. Ewels, P., et al., *MultiQC: summarize analysis results for multiple tools and samples in a single report*. *Bioinformatics*, 2016. **32**(19): p. 3047-8.
92. Chen, S., et al., *fastp: an ultra-fast all-in-one FASTQ preprocessor*. *Bioinformatics*, 2018. **34**(17): p. i884-i890.
93. Li, B. and C.N. Dewey, *RSEM: accurate transcript quantification from RNA-Seq data with or without a reference genome*. *BMC Bioinformatics*, 2011. **12**: p. 323.
94. Harrow, J., et al., *GENCODE: The reference human genome annotation for The ENCODE Project*. *Genome Research*, 2012. **22**(9): p. 1760-1774.
95. Dobin, A., et al., *STAR: ultrafast universal RNA-seq aligner*. *Bioinformatics*, 2013. **29**(1): p. 15-21.
96. Law, C.W., et al., *voom: Precision weights unlock linear model analysis tools for RNA-seq read counts*. *Genome Biol*, 2014. **15**(2): p. R29.
97. Herwig, R., et al., *Analyzing and interpreting genome data at the network level with ConsensusPathDB*. *Nat Protoc*, 2016. **11**(10): p. 1889-907.
98. Lopez-Otin, C., et al., *The hallmarks of aging*. *Cell*, 2013. **153**(6): p. 1194-217.
99. Kulkarni, A.S., S. Gubbi, and N. Barzilai, *Benefits of Metformin in Attenuating the Hallmarks of Aging*. *Cell Metab*, 2020.
100. Rayagiri, S.S., et al., *Basal lamina remodeling at the skeletal muscle stem cell niche mediates stem cell self-renewal*. *Nat Commun*, 2018. **9**(1): p. 1075.
101. Fry, C.S., et al., *Myogenic Progenitor Cells Control Extracellular Matrix Production by Fibroblasts during Skeletal Muscle Hypertrophy*. *Cell Stem Cell*, 2017. **20**(1): p. 56-69.
102. Hjorth, M., et al., *The effect of acute and long-term physical activity on extracellular matrix and serglycin in human skeletal muscle*. *Physiol Rep*, 2015. **3**(8).
103. Zhang, Q., et al., *Matrix metalloproteinase-2 plays a critical role in overload induced skeletal muscle hypertrophy*. *Muscles Ligaments Tendons J*, 2014. **4**(4): p. 446-54.
104. Welle, S., et al., *Skeletal muscle gene expression profiles in 20-29 year old and 65-71 year old women*. *Exp Gerontol*, 2004. **39**(3): p. 369-77.
105. Ubaida-Mohien, C., et al., *Discovery proteomics in aging human skeletal muscle finds change in spliceosome, immunity, proteostasis and mitochondria*. *Elife*, 2019. **8**.
106. Pan, Q., et al., *Deep surveying of alternative splicing complexity in the human transcriptome by high-throughput sequencing*. *Nat Genet*, 2008. **40**(12): p. 1413-5.

107. Ubaida-Mohien, C., et al., *Physical Activity Associated Proteomics of Skeletal Muscle: Being Physically Active in Daily Life May Protect Skeletal Muscle From Aging*. Front Physiol, 2019. **10**: p. 312.
108. Rodriguez, S.A., et al., *Global genome splicing analysis reveals an increased number of alternatively spliced genes with aging*. Aging Cell, 2016. **15**(2): p. 267-78.
109. Melov, S., et al., *Resistance exercise reverses aging in human skeletal muscle*. PLoS One, 2007. **2**(5): p. e465.
110. Kulkarni, A.S., et al., *Metformin regulates metabolic and nonmetabolic pathways in skeletal muscle and subcutaneous adipose tissues of older adults*. Aging Cell, 2018. **17**(2).
111. Snyman, C. and C.U. Niesler, *MMP-14 in skeletal muscle repair*. J Muscle Res Cell Motil, 2015. **36**(3): p. 215-25.
112. Bryer, S.C., et al., *Urokinase-type plasminogen activator plays essential roles in macrophage chemotaxis and skeletal muscle regeneration*. J Immunol, 2008. **180**(2): p. 1179-88.
113. Cathcart, J.M., et al., *Interleukin-6 increases matrix metalloproteinase-14 (MMP-14) levels via down-regulation of p53 to drive cancer progression*. Oncotarget, 2016. **7**(38): p. 61107-61120.
114. Yu, H., et al., *LIF negatively regulates tumour-suppressor p53 through Stat3/ID1/MDM2 in colorectal cancers*. Nat Commun, 2014. **5**: p. 5218.
115. Liu, L., et al., *Isolation of skeletal muscle stem cells by fluorescence-activated cell sorting*. Nat Protoc, 2015. **10**(10): p. 1612-24.
116. Juhas, M., et al., *Incorporation of macrophages into engineered skeletal muscle enables enhanced muscle regeneration*. Nat Biomed Eng, 2018. **2**(12): p. 942-954.
117. Kosmac, K., et al., *Immunohistochemical Identification of Human Skeletal Muscle Macrophages*. Bio Protoc, 2018. **8**(12).
118. Tarum, J., et al., *Electrical pulse stimulation: an in vitro exercise model for the induction of human skeletal muscle cell hypertrophy. A proof-of-concept study*. Exp Physiol, 2017. **102**(11): p. 1405-1413.
119. Scheler, M., et al., *Cytokine response of primary human myotubes in an in vitro exercise model*. Am J Physiol Cell Physiol, 2013. **305**(8): p. C877-86.
120. McLaughlin, S.L., et al., *NEDD9 depletion leads to MMP14 inactivation by TIMP2 and prevents invasion and metastasis*. Mol Cancer Res, 2014. **12**(1): p. 69-81.
121. Gramolelli, S., et al., *PROX1 is a transcriptional regulator of MMP14*. Sci Rep, 2018. **8**(1): p. 9531.
122. Spangenburg, E.E. and F.W. Booth, *Leukemia inhibitory factor restores the hypertrophic response to increased loading in the LIF(-/-) mouse*. Cytokine, 2006. **34**(3-4): p. 125-30.
123. Kosmac, K., et al., *Correlations of Calf Muscle Macrophage Content With Muscle Properties and Walking Performance in Peripheral Artery Disease*. J Am Heart Assoc, 2020. **9**(10): p. e015929.

124. Jensen, S.M., et al., *Macrophage Subpopulations and the Acute Inflammatory Response of Elderly Human Skeletal Muscle to Physiological Resistance Exercise*. Front Physiol, 2020. **11**: p. 811.
125. Miyatake, S., et al., *Contracting C2C12 myotubes release CCL2 in an NF-kappaB-dependent manner to induce monocyte chemoattraction*. Am J Physiol Endocrinol Metab, 2016. **310**(2): p. E160-70.
126. Oprescu, S.N., et al., *Temporal Dynamics and Heterogeneity of Cell Populations during Skeletal Muscle Regeneration*. iScience, 2020. **23**(4): p. 100993.
127. Rullman, E., et al., *A single bout of exercise activates matrix metalloproteinase in human skeletal muscle*. J Appl Physiol (1985), 2007. **102**(6): p. 2346-51.
128. Rullman, E., et al., *Endurance exercise activates matrix metalloproteinases in human skeletal muscle*. J Appl Physiol (1985), 2009. **106**(3): p. 804-12.
129. Pedersen, B.K. and M.A. Febbraio, *Muscles, exercise and obesity: skeletal muscle as a secretory organ*. Nat Rev Endocrinol, 2012. **8**(8): p. 457-65.
130. Broholm, C., et al., *Exercise induces expression of leukaemia inhibitory factor in human skeletal muscle*. J Physiol, 2008. **586**(8): p. 2195-201.
131. Lohi, J., et al., *Structural analysis and promoter characterization of the human membrane-type matrix metalloproteinase-1 (MT1-MMP) gene*. Gene, 2000. **242**(1-2): p. 75-86.
132. Welc, S.S., et al., *Targeting a therapeutic LIF transgene to muscle via the immune system ameliorates muscular dystrophy*. Nat Commun, 2019. **10**(1): p. 2788.
133. Murach, K.A., et al., *Fusion-Independent Satellite Cell Communication to Muscle Fibers During Load-Induced Hypertrophy*. Function (Oxf), 2020. **1**(1): p. zqaa009.
134. Ramaswamy, K.S., et al., *Lateral transmission of force is impaired in skeletal muscles of dystrophic mice and very old rats*. J Physiol, 2011. **589**(Pt 5): p. 1195-208.
135. Lindsey, M.L., et al., *Effect of a cleavage-resistant collagen mutation on left ventricular remodeling*. Circ Res, 2003. **93**(3): p. 238-45.
136. Fry, C.S., et al., *Regulation of the muscle fiber microenvironment by activated satellite cells during hypertrophy*. FASEB J, 2014. **28**(4): p. 1654-65.
137. Kulkarni, A.S., Peck, B.D., et al., *Metformin alters skeletal muscle transcriptome adaptations to resistance training in older adults*. Aging (Albany, NY). *In Press*

## VITA

### Personal Information

Name: Bailey Dakota Peck

Place of Birth: Charlotte, NC, USA

### Education

(Expected) 2020 University of Kentucky, Department of Rehabilitation Health Sciences, PhD Candidate

2016 University of North Carolina at Charlotte, Department of Exercise Science, M.S.

2014 University of North Carolina At Charlotte, Department of Exercise Science, B.S.

### Experience

2016-2020 Graduate Research Assistant, University of Kentucky, Peterson Lab

2014-2016 Graduate Research Assistant, University of North Carolina At Charlotte, Marino Lab

### Publications

Kulkarni AS, Peck BD\*, Walton RG, Kern PA, Mar JC, Windham ST, Bamman MM, Barzilai N, Peterson CA. Metformin alters skeletal muscle transcriptome adaptations to resistance training in older adults. *Aging (Albany)*. In press

Dungan CM, Peck BD, Walton RG, Huang Z, Bamman MM, Kern PA, Peterson CA. In vivo analysis of  $\gamma$ H2AX+ cells in skeletal muscle from aged and obese humans. *FASEB J*. 2020 Apr 4;. doi: 10.1096/fj.202000111RR. [Epub ahead of print] PubMed PMID: 32246795.

Walton RG, Dungan CM, Long DE, Tuggle SC, Kosmac K, Peck BD, Bush HM, Villasante Tezanos AG, McGwin G, Windham ST, Ovalle F, Bamman MM, Kern PA, Peterson CA. Metformin blunts muscle hypertrophy in response to progressive resistance exercise training in older adults: A randomized, double-blind, placebo-controlled, multicenter trial: The MASTERS trial. *Aging Cell*. 2019 Dec;18(6):e13039. doi: 10.1111/acer.13039. Epub 2019 Sep 26. PubMed PMID: 31557380; PubMed Central PMCID: PMC6826125.

Englund DA, Peck BD\*, Murach KA, Neal AC, Caldwell HA, McCarthy JJ, Peterson CA, Dupont-Versteegden EE. Resident muscle stem cells are not required for testosterone-induced skeletal muscle hypertrophy. *Am J Physiol Cell Physiol*. 2019 Oct 1;317(4):C719-C724. doi: 10.1152/ajpcell.00260.2019. Epub 2019 Jul 17. PubMed PMID: 31314585; PubMed Central PMCID: PMC6851003.

Peck BD, Brightwell CR, Johnson DL, Ireland ML, Noehren B, Fry CS. Anterior Cruciate Ligament Tear Promotes Skeletal Muscle Myostatin Expression, Fibrogenic Cell Expansion, and a Decline in Muscle Quality. *Am J Sports Med*. 2019 May;47(6):1385-1395. doi: 10.1177/0363546519832864. Epub 2019 Apr 17. PubMed PMID: 30995070.

Peck B, Renzi T, Peach H, Gaultney J, Marino JS. Examination of Risk for Sleep-Disordered Breathing Among College Football Players. *J Sport Rehabil.* 2019 Feb 1;28(2):126-132. doi: 10.1123/jsr.2017-0127. Epub 2018 Sep 29. PubMed PMID: 29035666.

Walton RG, Kosmac K, Mula J, Fry CS, Peck BD, Groshong JS, Finlin BS, Zhu B, Kern PA, Peterson CA. Human skeletal muscle macrophages increase following cycle training and are associated with adaptations that may facilitate growth. *Sci Rep.* 2019 Jan 30;9(1):969. doi: 10.1038/s41598-018-37187-1. PubMed PMID: 30700754; PubMed Central PMCID: PMC6353900.

Bennett JM, Marino JS, Peck B, Roos LG, Joseph KM, Carter LB, Smith CB, Rohleder N, Coffman MJ. Smokers Display Reduced Glucocorticoid Sensitivity Prior to Symptomatic Chronic Disease Development. *Ann Behav Med.* 2018 Sep 13;52(10):830-841. doi: 10.1093/abm/kax058. PubMed PMID: 30212844.

Kosmac K, Peck BD, Walton RG, Mula J, Kern PA, Bamman MM, Dennis RA, Jacobs CA, Lattermann C, Johnson DL, Peterson CA. Immunohistochemical Identification of Human Skeletal Muscle Macrophages. *Bio Protoc.* 2018 Jun 20;8(12). doi: 10.21769/BioProtoc.2883. PubMed PMID: 30148186; PubMed Central PMCID: PMC6105281.

Peck B, Huot J, Renzi T, Arthur S, Turner MJ, Marino JS. Mice lacking PKC- $\theta$  in skeletal muscle have reduced intramyocellular lipid accumulation and increased insulin responsiveness in skeletal muscle. *Am J Physiol Regul Integr Comp Physiol.* 2018 Mar 1;314(3):R468-R477. doi: 10.1152/ajpregu.00521.2016. Epub 2017 Nov 29. PubMed PMID: 29187383.

Long DE, Peck BD, Martz JL, Tuggle SC, Bush HM, McGwin G, Kern PA, Bamman MM, Peterson CA. Metformin to Augment Strength Training Effective Response in Seniors (MASTERS): study protocol for a randomized controlled trial. *Trials.* 2017 Apr 26;18(1):192. doi: 10.1186/s13063-017-1932-5. PubMed PMID: 28441958; PubMed Central PMCID: PMC5405504.

Hinds TD, Peck B, Shek E, Stroup S, Hinson J, Arthur S, Marino JS. Overexpression of Glucocorticoid Receptor  $\beta$  Enhances Myogenesis and Reduces Catabolic Gene Expression. *Int J Mol Sci.* 2016 Feb 11;17(2):232. doi: 10.3390/ijms17020232. PubMed PMID: 26875982; PubMed Central PMCID: PMC4783964.

Turner MJ, Guderian S, Wikstrom EA, Huot JR, Peck BD, Arthur ST, Marino JS, Hubbard-Turner T. Altered left ventricular performance in aging physically active mice with an ankle sprain injury. *Age (Dordr).* 2016 Feb;38(1):15. doi: 10.1007/s11357-016-9877-2. Epub 2016 Jan 23. PubMed PMID: 26803818; PubMed Central PMCID: PMC5005884.

\*Indicates Co-First Author